2-P

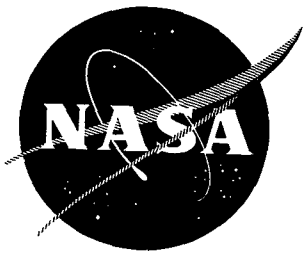

NASA CR 120982
MTI-72TR33

HIGH PRESSURE PULSED-CAPILLARY VISCOMETRY

by

Richard L. Smith
Jed A. Walowit
C.H.T. Pan

MECHANICAL TECHNOLOGY INCORPORATED

Prepared for

NATIONAL AERONATUICS AND SPACE ADMINISTRATION

NASA—Lewis Research Center

Contract NAS3-14419

W.J. Anderson — Chief, Bearings Branch

1. Report No.	2. Government Accession No.	3. Recipient's Catalog No.
CR 120982		

4. Title and Subtitle	5. Report Date
HIGH PRESSURE PULSED CAPILLARY VISCOMETRY (U)	8/17/72
	6. Performing Organization Code
7. Author(s)	8. Performing Organization Report No.
R.L. Smith, J.A. Walowit, C.H.T. Pan	MTI 72TR33
	10. Work Unit No.
9. Performing Organization Name and Address	
Mechanical Technology Incorporated 968 Albany-Shaker Road Latham, New York 12110	11. Contract or Grant No. NAS3-14419
	13. Type of Report and Period Covered
12. Sponsoring Agency Name and Address	Contractor Report
National Aeronautics and Space Administration Washington, D.C. 20546	14. Sponsoring Agency Code

15. Supplementary Notes

Project Manager, W.J. Anderson, Chief, Bearings Branch
NASA Lewis Research Center, Cleveland, Ohio

16. Abstract

An analytical and test program was conducted in order to establish the feasibility of a multi-chamber pulsed-capillary viscometer. The initial design incorporated a piston, ram, and seals which produced measured pulses up to 30,000 psi (206,800 NT/M^2) in the closed chamber system. Pressure pulses from one to ten milliseconds were investigated in a system volume of 1 in^3 (1.63×10^{-5} M^3).

Four test fluids: a MIL-L-7808, a 5P4E polyphenyl ether, a MIL-L-23699A, and a synthetic hydrocarbon were examined in the test pressure assembly. The pressure-viscosity coefficient and viscosity delay time were determined for the MIL-L-7808 lubricant tested.

17. Key Words (Suggested by Author(s))	18. Distribution Statement
Viscometry Pressure-viscosity coefficients Capillary Viscometer	Publicly available

19. Security Classif. (of this report)	20. Security Classif. (of this page)	21. No. of Pages	22. Price*
Unclassified	Unclassified	60	~~$3.00~~ $3.25

* For sale by the National Technical Information Service, Springfield, Virginia 22151

FOREWORD

The investigation reported herein was performed by Mechanical Technology Incorporated in fulfillment of Contract NAS3-14419 for the National Aeronautics and Space Administration, Lewis Research Center, Cleveland, Ohio. Mr. William J. Anderson was the NASA Project Manager.

ABSTRACT

An analytical and test program was conducted in order to establish the feasibility of a multichamber pulsed-capillary viscometer. The initial design incorporated a piston, ram, and seals which produced measured pulses up to 30,000 psi (206,800 NT/M^2) in the closed chamber system. Pressure pulses from one to ten milliseconds were investigated in a system volume of 1 in^3 (1.63×10^{-5} M^3).

Four test fluids: a MIL-L-7808, a 5P4E polyphenyl ether, a MIL-L-23699A, and a synthetic hydrocarbon were examined in the test pressure assembly. The pressure-viscosity coefficient and viscosity delay time were determined for the MIL-L-7808 lubricant tested.

TABLE OF CONTENTS

LIST OF FIGURES

LIST OF FIGURES (Continued)

LIST OF TABLES

INTRODUCTION

The operation of rolling element bearings and other high speed concentrated contact elements such as cams, gears, and rolling contact drives involves subjecting lubricants to extremely high pressures of the order of hundreds of thousands of psi and high shear rates for very short duration times. Many investigations have been performed to attempt to understand the behavior of lubricants under these conditions. Such investigations include:

1. High pressure viscometry which provides measurements of lubricant viscosity under high pressures and nearly isothermal conditions and at low shear rates and long times.

2. Rolling-sliding contact measurements which involve obtaining traction and film thickness data with a highly loaded rolling disc machine or other type of rolling contact apparatus. Here the lubricant is subjected to high pressures as well as high shear rates, short times and often high temperature rises.

This second class of measurements does simulate the conditions undergone in concentrated contact elements. However, they simulate all of the conditions simultaneously (high pressures, high temperatures, high shear rates and short times) with a geometry that is somewhat uncertain in that the film thickness is determined by the lubrication process itself and must be measured.

The results of these rolling contact measurements indicate at the high speeds encountered in a concentrated contact element, various phenomena occur that are not explainable by high shear rate and thermal effects alone. In particular, variations of measured traction and film thickness with rolling speeds can not be accounted for by long time equilibrium Newtonian theory nor can they be described by simple shear rate dependent lubricant models. It has been hypothesized that short time effects could be responsible for some of these observations. In particular, a lubricant moving at a thousand inches per second will pass through a 10 mil contract zone with a residence time of 10 microseconds. During this passage through the contact zone a particle of fluid will experience a change in pressure from ambient to hundreds of thousands of psi and back to ambient. It has been hypothesized that the viscosity which increases radically with pressure during long times does not increase quite as radically during short times. In other words, there is a delay time associated with the response of the viscosity to a rapid change in pressure. This viscosity delay phenomenon is the subject of the present investigation.

In order to study viscosity delay phenomenon, a simple apparatus consisting of a pulsed capillary viscometer has been developed. A pressure pulse is transmitted to a reservoir full of fluid and a small amount of fluid is forced through a capillary to another closed reservoir full of fluid. By measuring the pressure time characteristics of both reservoirs it is possible to infer the viscous characteristics of the fluid. Pulse times can readily be achieved to the order of a few milliseconds and residence times in the capillary tube can be as small as a few microseconds. The capillary tube can be built to

have a relatively short length and small but controlled radius hence providing a controlled geometry. It was hoped that this device could provide a simplified means of measuring viscosities under moderately high pressures and short times but at lower shear rates with smaller thermal effects than encountered in rolling contact apparatus. Hence, it is that the pulse type viscometer will have the advantage over the disc machine type of apparatus in that it provides a controlled geometry and at least partially isolates the short time effects from high shear rate effects in a relatively simple apparatus.

The following sections describe the concept of the pulse viscometer, the analyses required to relate pressure pulse measurements to viscosity, viscosity-pressure and viscosity-time characteristics, a description of experiments that have been performed together with results of a viscometric analysis of the test data.

THE PULSED-CAPILLARY VISCOMETER

Conceptual Discussion

High pressure viscometers (1) which incorporate capillary tubing as flow restrictors have been in use since 1966. Viscometers incorporating capillary tubes in the past have been of the slow flow variety. Fluid under high static pressure is induced to flow between two chambers via capillary tubing under a relatively small differential pressure.

The present design incorporates two or more chambers which are initially unpressureized and connected by capillary tubing to the largest volume chamber. The design concept is shown schematically in Figure 1. The design is unique in that flow through the capillary tube is produced when the primary chamber V_1 is pressurized momentarily by impacting the enclosure piston. Each chamber of the viscometer contains an active pressure transducer element which provides a readout of the pressure-time history within each cavity of the high-pressure system. An oscilloscope display of a typical pair of pressure pulses from a single impact is shown schematically in Figure 2. The impact is produced in such a way as to provide a half-sine wave pressure-time pulse in the primary chamber of the viscometer. The pressure buildup as a function of time in the secondary chamber is characteristic of the rheological properties of the contained fluid in the closed system. Correct sizing of volume V_2 and the capillary tubing leading to the primary chamber provides the proper readout sensitivity for the viscosity of any fluid chosen for investigation.

Capillary tubes which are too large will allow the secondary pressure (p_2) to follow the primary pressure (p_1) and no estimate of fluid test viscosities could be made. Conversely, capillaries which are too small will not allow sufficient fluid to enter the secondary chamber during an applied pressure pulse and no signal would be obtained from the secondary chamber. Proper sizing of the capillary tubes is required for the desired output sensitivity and can be estimated from the approximate test fluid viscosity under investigation.

The relative size of the test volumes, V_1 and V_2, as shown in Figure 1 is also important when considering the desired range of pressure ratios p_2/p_1 (see Figure 2). If V_2 is too large, the filling time will be extremely long and will not provide sufficient pressure buildup in the secondary chamber. A small volume V_2 would create a condition similar to an extremely large capillary in that the pressure ratio p_2/p_1 would be one and the instrument would provide no usable information.

A consideration of the base viscosity of the test fluids is necessary to determine the proper secondary chamber and capillary sizes. Highly viscous fluids will reduce pressure buildups in the secondary chamber as a result of reduced flow. On the other hand, fluids with low viscosities might not be flow resistant enough when passing through improperly sized capillaries and would provide little or no viscosity readout by allowing (p_2) to follow (p_1) too closely.

Properly sized chambers and capillaries for the expected fluids to be tested

will yield a peak pressure in the secondary chamber which is one-half or less of the peak value attained from a pulse applied to the primary chamber. The analysis described in detail in the following section prescribes the parametric interdependence for the high-pressure pulsed-capillary viscometer and gives an insight into how one can properly size chamber components for correct sensitivity.

Test Assembly and Data

Although the test approach used in measuring viscosities with pulsing techniques is new, the test apparatus is a combined assembly of commercially available and new machined components. The nature of the physical requirements dictated specific design features which were chosed for testing and are reviewed in this section.

Primary Pressure Chamber

The primary chamber (Volume V_1 in Figure 1) is contained in a commercially available cylinder capable of withstanding static pressures up to 200,000 psi. The test cylinder was constructed of two prestressed walls and has a six inch outside diameter and a five-eighths inch bore. The piston ram during operation drives a floating seal and plunger into the bore of the chamber. The standard seal used in the plunger was replaced with an elastomeric O-ring in order to ensure a positive seal with a minimum of sliding friction. Visual evidence of sealing (at least to the pulsed 30,000 psi pressure level) was shown by the return of the piston to its original height after every impact. Perfect sealing of the primary chamber was not necessary for operation since the primary pressure buildup was monitored during pulses.

Capillary Tubes and Secondary Chambers

The theory of the pulsed viscometer concept (to be described later) provides a dimensionless parameter β which prescribes appropriate dimensions of the capillary and secondary chamber combinations. An appropriate combination of parameters requires that $\beta < 1$ for proper sensitivity where

$$\beta = \frac{\pi R^4 kT}{8 \mu L V_2} \tag{1}$$

The diameter of the capillary tubes used in the high-pressure tests was determined experimentally from a set of low pressure flow tests. The integrally mounted capillary and associated secondary chamber was calibrated by forcing water through the tubing. Measurement of the flow rates of distilled water through the known length of capillary tubing provided an accurate determination of the radius of the capillary tubing. In addition, volumetric determination of the test secondary chambers from machined dimensions provided the remaining information required to evaluate the geometric portion of β defined below:

$$\text{geometry factor} = \frac{\pi R^4}{8 L V_2}$$

for each test setup used in obtaining the oscilloscope pressure data presented in this report. The calibration for each test capillary indicated

Test Capillary Designation	Non-Dimensional Geometry Factor
A	2.027×10^{-8}
B	3.544×10^{-8}
C	1.418×10^{-9}
D	1.229×10^{-9}
E	1.893×10^{-9}

Test capillary tubes were produced from sectioning standard stainless steel hypodermic tubing. Lengths varied from .100 to .400 inches and the inside diameter from 4 to 8 mils. The securing of the tubing in line between chambers was accomplished with heat cured epoxy and worked well over the pressure range tested in the present program.

The primary pressure chamber contained approximately one cubic inch of test lubricant. A determination of the precise volume was not important as long as the primary chamber volume was at least twenty times greater than the secondary volume. The primary chamber in the present study was 25 to 100 times that of the secondary volume depending upon the initial position of the piston ram.

Pressure Gages

Two types of pressure gages were tested during this program. Both were made of manganin sensing elements, one in the form of a wire wound open coil and the other in the form of a thin 200 micro-inch foil. Although each type of sensor was available commercially, each type had to be modified slightly for mounting on the secondary chamber follower and seal.

Figure 3 shows a mounted coil of the wire type sensor ready for operation. A second coil identical to the one shown was mounted externally to the pressure chamber to form a half-bridge in a standard Wheatstone arrangement. When mounted in the Wheatstone bridge, each sensor provided a 100 millivolt output at 10,000 psi pressure. The resolution of the oscilloscope pressure-time trace, as a result, was limited to $\pm$ 25 psi. Pulse periods from two to ten milliseconds were determined with an accuracy of 5 percent or better from the oscilloscope tracings.

Foil gages made of manganin were also evaluated for pulsed pressure determination. The foil was an open etched pattern 200 microinches thick and had an active grid area of approximately 1/8 inch square when bonded to the chamber follower as seen sectionally in Figure 4. Again the output sensitivity of the element was adjusted to be the same as the wire type gage and was statically calibrated with the aid of a hand pump at 10,000 psi in a closed pressure chamber. A standard Bourdon tube pressure gage with 10,000 psi scale and a $\pm$ 1 percent accuracy was used for calibrating the pressure detection bridge.

Of the two types of active pressure elements used, the foil gage was preferred for its small size and minimum volumetric displacement. It is possible that a modified version of the foil pressure sensor could be incorporated within a capillary channel if analytical evidence was produced to require such a measurement.

Instrumentation

A schematic of the instrumentation setup is presented in Figure 5. The simplicity of the pulsed pressure viscometer is apparent from the diagram. The essential components are pressure transducer elements, Wheatstone bridges, and a multi-beam oscilloscope with camera attached. Photographs of Figures 6 and 7 show the bridge instrumentation and the high-pressure cylinder. Each bridge contains its own zero balance control and amplifier with span adjust for calibrated voltage output. The input connections of the bridges used allowed hookup for either two or four external bridge arm connections. The signal to noise ratio for the smallest pressures measured was 20:1 whereas the ratio went to a 1000:1 for the higher pressure signals detected. The frequency response of the bridge system was limited to the zero to twenty thousand cycles per second range in the present facility. The necessary bridge frequency response for the shortest pulses induced in the present study was one thousand cycles per second. A full list of instruments used and their model numbers are included in Appendix 1 for further reference.

Test Data

The output data from the present test program is contained in over one hundred and fifty dual trace pressure-versus-time oscilloscope photographs. Pressure-time traces for each of four fluids were recorded. The evaluated fluids were

Fluid	Description
MIL-L-7808	Humble #2389
Polyphenyl Ether	Monsanto OS-124
MIL-L-23699A	Mobil Jet II
Synthetic Hydrocarbon	XRM 214B

and some of their physical properties as determined from investigations performed prior to the present study are included in Appendix 2.

In addition to determining chamber pressures during test impact, checks were made of the test fluid compressive heating with the aid of small thermocouples. Two five-mil diameter thermocouples were joined and flattened to less than a 2-mil thickness. Stepped thermal changes applied to the produced thermocouples revealed a response time of approximately three milliseconds. Using the miniature temperature sensors, the bulk compressive heating within the secondary and primary chambers were found to be less than $4^{o}F$ for applied pressure pulses of approximately 20,000 psi, lasting from 5 to 6 milliseconds.

Viscosity data are inferred analytically from the pressure-time traces obtained from the primary and secondary chambers after impact. Typical pairs of traces obtained for each lubricant tested are displayed in Figures 8 through 31. The pressure (p_1) of the impact load is found in each run from the upper trace, depicted in each photograph. Since the scale factors vary from picture to picture, the peak pressure in the primary chamber ($p_{1\ max}$) and the peak pressure in the secondary chamber ($p_{2\ max}$) are noted at the side of each run shown.

PULSE VISCOMETER ANALYSIS

Pulse viscometry measurements consist of input temperatures, times, pressures, and geometric variables including reservoir volumes and capillary lengths and diameters. In order to convert these measurements into fluid properties, it is essential that analyses be performed which relate fluid properties (mainly the viscosity and the viscosity pressure, temperature, and time characteristics) to these pressure measurements.

The analyses to be presented here are divided into two basic parts. The first of these represents a development of simplified relationships assuming highly idealized viscosity-pressure-temperature relationships and no time effects which has been used for purposes of designing the test apparatus and extracting basic preliminary information about the relationship and sensitivity between measured pulses and long-time viscosity characteristics. The second set of analyses is somewhat more comprehensive in that it allows for a viscosity delay, it allows for an arbitrary input viscosity-pressure-temperature relationship (for equilibrium viscosity), and allows for other variable properties such as bulk modulus variations with pressure.

The first set of analyses thus provides qualitative trends and ranges of relevance for the various parameters as well as identifying relevant parameters. The second set of analyses provides a more sophisticated tool for extraction of viscosity and viscosity delay characteristics.

Simplified Analyses for Predicting Long-Time Pulse Measurements

A schematic showing the two reservoirs, noted as reservoirs 1 and 2 for inlet and exit ends of the capillary respectively, are shown in Figure 22. A pulse is imparted to reservoir 1 which acts as a spring, providing an approximately sinusoidal pressure pulse which forces fluid through the capillary into reservoir 2. In this section the flow through the capillary and the resulting pressure profile, p_2 (t), will be analyzed first for an isoviscous fluid and then extended to include viscosity-pressure and viscosity-temperature effects.

Isoviscous Fluid

The volumetric flow rate, Q, of an isoviscous fluid undergoing laminar flow through a capillary is given by

$$Q = \frac{\pi R^4}{8\mu} \frac{(p_1 - p_2)}{L} \tag{2}$$

If the density pressure relationship is of the form

$$\rho = \rho_o \left(1 + \frac{p}{k}\right) \tag{3}$$

where k is the bulk modulus of the fluid and $p/k < 1$ (.2 or less) then the pressure, p_2, is related to the flow, Q, by

$$\frac{dp_2}{dt} = \dot{p}_2 = \frac{kQ}{V_2} \tag{4}$$

If the input pressure (p_1) is of the form

$$p_1 = \begin{cases} af(t/t_o), & t < t_o \\ 0 \quad , & t > t_o \end{cases} \tag{5}$$

where t_o denotes the duration time of the impulse and f is a dimensionless input pressure function then we may combine Equations (1), (2), and (5) to obtain the relationship

$$\frac{dp_2}{dt} = \frac{\pi R^4 k}{8\mu L V_2} [af(t/t_o) - p_2] \qquad 0 < t < t_o \tag{6}$$

Now introduce dimensionless variables

$$\tilde{p}_2 = p_2/a \qquad \text{and} \qquad \tau = t/t_o$$

and the parameter

$$\beta = \frac{\pi R^4 k t_o}{8\mu L V_2}$$

to obtain the dimensionless equation

$$\frac{d\tilde{p}_2}{d\tau} = \begin{cases} \beta\{[f(\tau) - \tilde{p}_2]\}, & 0 < \tau < 1 \\ -\beta\tilde{p}_2 \quad , & \tau > 1 \end{cases} \tag{7}$$

$$\tilde{p}_2(0) = 0$$

The above first order equation has the solution

$$\tilde{p}_2 = \beta \int_o^{\tau} e^{-\beta(\tau-\tau')} f(\tau')d\tau' \quad , \qquad \tau \leq 1$$

$$\tilde{p}_2 = \beta e^{-\beta\tau} \int_o^{1} e^{\beta\tau'} f(\tau')d\tau \quad , \qquad \tau \geq 1 \tag{8}$$

If mechanical energy, E, is imparted to a system of mass, M (M would be the mass of the piston if the projectile did not stick to the piston during the pulse time or the sum of the masses of the piston + projectile if sticking did occur), then the pulse pressure would be

$$p_1 = \sqrt{\frac{2kE}{V_1}} \sin\sqrt{\frac{kA^2}{MV_1}}\, t \tag{9}$$

where A denotes the cross sectional area of the piston. The above formula neglects sonic effects, assumes no leakage, and is strictly valid for $V_1 >> V_2$. Equation (9) was arrived at by considering a simple spring and mass system. An initial velocity v_o is imparted to the system given by $v_o = \sqrt{2E/M}$. If the piston displaces a distance x, the volume displaced would be $\Delta V_1 - Ax$ and for small displacement $-\Delta V_1/V_1 \approx \Delta\rho/\rho_o = p/k$. The right hand side of the above equation is a consequence of Equation (3). The spring stiffness S would then be given by $S = Ap/x = RA^2/V_1$. Equation (9) thus represents the simple spring and mass solution for a system having mass M, stiffness S given as initial velocity v_o given by the above expressions. The amplitude of the pressure pulse is

$$a = \sqrt{\frac{2kE}{V_1}} \tag{10}$$

and the period is

$$t_o = \pi\sqrt{\frac{MV_1}{kA^2}} \tag{11}$$

hence

$$f(\tau) = \sin \pi\tau \tag{12}$$

The solution to Equation (8) with $f(\tau) = \sin\pi\tau$ is

$$\tilde{p}_2 = \begin{cases} \dfrac{\beta}{\pi^2 + \beta^2}\left(\beta\sin\pi\tau - \pi\cos\pi\tau + \pi e^{-\beta\tau}\right) & 0 \le \tau \le 1 \\ \dfrac{\pi\beta(1+e^{-\beta})e^{-\beta(\tau-1)}}{\pi^2 + \beta^2} & \tau > 1 \end{cases} \tag{13}$$

The value of τ for which $\tilde{p}_2$ is maximum is given by the solution to

$$\beta\left(e^{-\beta\tau_{max}} - \cos\pi\tau_{max}\right) = \pi\sin\pi\tau_{max} \tag{14}$$

Values of τ_{max} calculated from Equation (14) along with corresponding values of p_{max} are shown in Figure 23. It can be seen that for greatest sensitivity of measured pressure, p_2, to viscosity, the parameter, β, should be considerably less than one.

The Effect of Viscosity-Pressure Dependence

If the viscosity varies with pressure in accordance with the relationship

$$\mu = \mu_o g(p)$$

then Equation (1) assumes the form

$$Q = \frac{\pi R^4}{8\mu_o L} \int_{p_2}^{p_1} \frac{dp}{g(p)} \tag{15}$$

and Equations (4), (5), and (15) may be solved simultaneously. If we assume a viscosity-pressure relationship of the form

$$g(p) = e^{\alpha p} \tag{16}$$

where α is the conventional pressure coefficient of viscosity then Equation (15) becomes

$$Q = \frac{\pi R^4}{8\mu_o L} (e^{-\alpha p_2} - e^{-\alpha p_1}) \tag{17}$$

and the differential equation for $\tilde{p}_2$ is as follows

$$\frac{d\tilde{p}_2}{d\tau} = \begin{cases} \frac{\beta}{\tilde{\alpha}} (e^{-\tilde{\alpha}\tilde{p}_2} - e^{-\tilde{\alpha} f(\tau)}), & 0 < \tau \leq 1 \\ \frac{\beta}{\tilde{\alpha}} (e^{-\tilde{\alpha}\tilde{p}_2} - 1), & \tau > 1 \end{cases} \tag{18}$$

$$\tilde{p}_2(0) = 0$$

where the parameter $\tilde{\alpha}$ is defined by $\tilde{\alpha} = \alpha a$.

The above equation may be put into linear form with the transformation

$$\emptyset = e^{\tilde{\alpha}\tilde{p}_2} \tag{19}$$

as follows

$$\frac{d\phi}{d\tau} = \begin{cases} \beta(1 - \phi e^{-\tilde{\alpha} f(\tau)}) , & 0 < \tau \leq 1 \\ \beta(1 - \phi) & \tau > 1 \end{cases} \tag{20}$$

Equation (20) has been solved numerically for ϕ for $f(\tau) = \sin\pi\tau$. Maximum values of $\tilde{p}_2$ are plotted against β for various values of $\tilde{\alpha}$ in Figure 24.

An asymptotic expression has also been obtained for the solution to Equation (20) in the interval $0 < \tau < 1$ based upon large values of the parameters $\tilde{\alpha}$ and $\tilde{\alpha}\pi/\beta$. The resulting expression for ϕ is

$$\phi = 1 + \beta\tau - \frac{\beta}{\tilde{\alpha}\pi}\left[1 - e^{-\alpha\pi\tau} + (1 + \beta)e^{-\tilde{\alpha}\pi(1-\tau)}\right] \tag{21}$$

and the maximum value of ϕ occurs at

$$\tau_{max} = 1 - \frac{\ell n\left|\frac{1 + \beta}{\tilde{\alpha}\pi}\right|}{}$$

Hence, for the major portion of the pulse duration ϕ will be linear with τ.

If β is small and $\tilde{\alpha}$ is large then p_2 will approach the form

$$p_2 = \frac{\pi R^4 k}{12\mu_o \alpha L V_2} t, \qquad 0 < t < T$$

hence, p_2 will depend upon the product of the base viscosity (μ_o) and the pressure coefficient of viscosity (α) which is similar to the dependence predicted for film thicknesses in elastohydrodynamic contacts.

Inclusion of Thermal Effects

The nonintegrated form of Equation (15) that is valid when μ varies with axial position, z, but does not vary with radial position, r, is obtained simply by replacing $(p_1-p_2)/L$ appearing in Equation (2) by -dp/dz

Hence,

$$Q = -\frac{\pi R^4}{8\mu}\frac{dp}{dz} \tag{22}$$

and the average velocity, $\bar{u}$, is given by

$$\bar{u} = \frac{Q}{\pi R^2} = -\frac{R^2}{4\mu}\left(\frac{dp}{dz}\right) \tag{23}$$

The volumetric rate of power dissipation due to viscous heating (neglecting radial dependence on μ) is given by

$$\Phi_v = \mu \left(\frac{\partial u}{\partial r}\right)^2 = \frac{r^4}{4\mu} \left(\frac{dp}{dz}\right)^2$$

Hence, the heat generated per unit length Φ_L is given by

$$\Phi_L = 2\pi \int_0^R r \Phi_v \, dr = \frac{\pi R^4}{8\mu} \left(\frac{dp}{dz}\right)^2 \tag{24}$$

If the average rate of heat generated per unit length is equated to the rate of removal by convection then

$$\rho c Q \frac{dT}{dz} = \Phi_L$$

and when $\bar{u}$ and Φ_L are replaced by Equations (23) and (24) the resulting expression is

$$\rho c \frac{dT}{dz} = \frac{dp}{dz}$$

which may be integrated to yield the equation

$$T = T_1 + \frac{p_1 - p}{\rho c} \tag{25}$$

where T_1 denotes the temperature in reservoir 1.

Equation (25) thus indicates that subject to the limitations imposed by radial averaging and the assumed modes of heat generation and removal the temperature rise depends only on the heat capacity and the local pressure drop and is otherwise independent of viscosity and geometry.

If the viscosity varies with pressure and temperature in accordance with the relationship

$$\mu = \mu_o g^* (p,T) \tag{26}$$

then the effect of temperature variations may be accounted for by replacing Equation (15) with

$$Q = \frac{\pi R^4}{8\mu_o L} \int_{p_2}^{p_1} \frac{dp}{g^*\left(p, T_1 + \frac{p_1 - p}{\rho c}\right)} \tag{27}$$

In the special case

$$\mu = \mu_1 e^{\alpha p - \delta(T - T_1)} \tag{28}$$

The denominator in the integrand in Equation (27) assumes the form

$$g^*(p, T_1 + \frac{p_1 - p}{\rho c}) = \mu_o e^{\frac{\delta p_1}{\rho c}} e^{(\alpha + \frac{\delta}{\rho c})p}$$

and the differential equation for pressure analogous to Equation (18) becomes

$$\frac{d\tilde{p}_2}{d\tau} = \frac{\beta}{(\tilde{\alpha} + \tilde{\delta})} \left[e^{-(\tilde{\alpha} + \tilde{\delta})\tilde{p}_2 + \tilde{\delta} f(\tau)} - e^{-\tilde{\alpha} f(\tau)} \right], \quad 0 < \tau \leq \tau_{max} \tag{29}$$

where the parameter $\tilde{\delta}$ is defined as

$$\tilde{\delta} = \frac{\delta a}{\rho c} \tag{30}$$

Hence, with the use of the viscosity temperature model given by Equation (28) it is possible to represent the maximum pressure ratio ($\tilde{p}_{2max}$) as functions of the three parameters $\beta, \tilde{\alpha}$, and $\tilde{\delta}$. Curves showing the variation of $\tilde{p}_{2max}$ with β at various values of $\tilde{\alpha}$ and $\tilde{\delta}$ are given in Figures 25 through 27.

It can be seen from Figures 25 through 27 that in all cases $\tilde{p}_{2max}$ becomes insensitive to β as β becomes large. In that β is the sole parameter reflecting the viscosity at ambient pressure it is essential that significant sensitivity with respect to β prevail, hence, based upon these figures one should design the apparatus with values of β somewhat less than one. The practical range of parameters $\tilde{\alpha}$ and $\tilde{\delta}$ for present test conditions with present lubricants should be between 0 and 3 for both parameters. Bearing this in mind, it is possible to use Figures 25 through 27 to design the test apparatus so that necessary ranges of operation are encountered where β is sufficiently small to provide sensitivity to viscosity yet large enough to provide measurable values of p_2.

In order to more rigorously extract viscosities and viscosity delay information, one should have an analysis that incorporates the best available viscosity temperature and viscosity pressure data and bulk modulus data along with an inclusion of the effects of a viscosity delay. In the following section such an analysis is developed.

Refined Analysis Including Viscosity Delay Effects

Viscosity Delay Mechanism

A first order lower viscosity delay mechanism has been used to quantify and extract time effects from the apparatus.

Suppose at time t = 0 a fluid previously existing under pressure, p_a, is

suddenly exposed to pressure, p_b. If the long-time equilibrium viscosity-pressure relationship is denoted by $\mu_e(p)$, then the instantaneous fluid viscosity is assumed to rise at a rate which is proportional to the departure from equilibrium in accordance with the first order rate equation

$$\frac{d\mu}{dt} = \frac{\mu - \mu_e (p_b)}{t_d} \tag{31}$$

where the constant t_d has dimensions of time and will be referred to as the fluid delay time.

The solution to Equation (31) subject to the initial condition $\mu = \mu_e(p_a)$ at $t = 0$ is

$$\mu = \mu_e(p_b) - [\mu_e(p_b) - \mu_e (p_a)]e^{-t/t_d} \tag{32}$$

of the variation of μ with time in accordance with Equation (32) is shown schematically in Figure 28.

Since viscosity is a function of temperature as well as pressure, it is necessary to hypothesize a model for the time response due to a sudden change in temperature. For the present time, it will be assumed that viscosity responds instantaneously to temperature and our attention will be confined primarily to the delay associated with a rapid change in pressure.

We will confine our attention to an equilibrium viscosity-pressure-temperature relationship of the form

$$\mu_e = \mu_o \; G_e (p) \; F (T) \tag{33}$$

where μ_o is the equilibrium viscosity at ambient pressure and reference temperature T_o and G_e represents the pressure portion of the equilibrium (long-time) viscosity function and F(T) reflects the temperature variation in viscosity.

The instantaneous viscosity μ is given by

$$\mu = \mu_o \; G(p) \; F(T) \tag{34}$$

where G (p) is assumed to follow a first order delay law analogous to Equation (31)

$$\frac{dG}{dt} = - \frac{(G - G_e)}{t_d} \tag{35}$$

and F(T) is assumed independent of time.

Equations for Predicting Effects of Viscosity Delay on Pressure Measurements

Equation (35) provides the necessary relationship for predicting viscosity delay effects in reservoir 1 where the fluid experiences a pressure pulse, p_1 (t), applied over a duration of time, t_o.

Hence, in reservoir 1 and at the entrance to the capillary (z = 0) the viscosity delay equation is

$$\frac{dG_1}{dt} = - \frac{(G_1 - G_e(p_1)}{t_d(p_1)} , \qquad \begin{matrix} x = 0 \\ 0 < t < t_o \end{matrix} \tag{36}$$

where the subscript 1 denotes reservoir 1.

Equation (36) applies to μ as well as G here since compressive heating is small and there is no significant shear heating in the reservoirs. Hence, the reservoirs should be very nearly isothermal at temperature T_1.

In the capillary, however, a particle of fluid passes through a pressure field and the time derivative, d/dt, is replaced by the "total derivative" u d/dx. If one again replaces the radially-varying velocity, u, with the average value, $\bar{u}$, as defined in Equation (23), the delay equation in the capillary becomes

$$\bar{u} \frac{\delta G}{\delta z} = - \frac{G - G_e(p)}{t_d(p)} , \qquad 0 < z < L \tag{37}$$

The flow rate Q is again related to the pressure buildup in reservoir 2 $\dot{p}_2$ by Equation (4) and is applicable to a variable as well as constant bulk modulus. When the flow rate given by Equation (4) is equated to that given by Equation (22) and the resulting equation is solved for the pressure gradient, the following expression is obtained

$$\frac{\delta p}{\delta z} = - \frac{8\mu V_2 \dot{p}_2}{\pi R^4 k(p_2)} , \qquad 0 < z \leq L, \quad t > 0 \tag{38}$$

The average velocity, $\bar{u}$, appearing in Equation (37) is expressed in terms of $\dot{p}_2$ in accordance with Equation (4) to obtain the differential equation

$$\dot{p}_2 \frac{\delta G}{\delta z} = - \frac{\pi R^2}{V_2} \frac{k(p_2)}{t_d(p)} [G - G_e (p)] , \qquad 0 < z \leq L \tag{39}$$

The temperature profile in the capillary resulting from viscous heating is still related to pressure by Equation (25), hence, the viscosity μ appearing in Equation (38) may be expressed in terms of G and p as

$$\mu = \mu_1 G(p) F[p_1 - \rho c (T - T_1)] \tag{40}$$

The reference temperature, T_o, has now been taken to be the inlet reservoir temperature, T_1.

At each instant of time, Equations (38) through (40) constitute a nonlinear second order system with two dependent variables (G and p) and one independent variable z. The equations also contain one unknown parameter $\dot{p}_2$.

The pressure, p_1, is a measured input variable which is either interpolated from a table or approximated with a sinusoidal input function. Other input quantities are geometric parameters R, L, and V_2, viscosity functions G_e (p) and F(T), bulk modulus function k(p) and delay time function $t_d(p)$. The principal output quantity will be the pressure p_2.

Equation (36) may be solved numerically by the fourth order Runge-Kutta process subject to the boundary condition at t = 0, G = 1 to obtain G_1 as a function of t.

There are three constraints on the second order system given by Equations (38) through (40). The first two of these are the conditions at x = 0

$$G = G_1, \quad p = p_1 \quad \text{at } x = 0 \tag{41}$$

The third condition at x = L is

$$p = p_2 \quad \text{at } x = L \tag{42}$$

which determines $\dot{p}_2$.

Equations (38) through (40) are solved numerically at each time step with the fourth order Runge-Kutta process. The value of $\dot{p}_2$ is varied systematically in a nesting procedure until Equation (42) is satisfied. The value of p_2 at the next time increment is obtained with the central difference formula

$$p_2(t_{n+1}) = 2\Delta t\, \dot{p}_2\,(t_n) - p_2\,(t_{n-1})$$

A time sharing computer program is available for solving the above equations to any reasonable degree of accuracy for any given set of input functions and parameters.

Results of Viscosity Delay Computations

In order to qualitatively illustrate the effect of viscosity delay and to estimate the sensitivity of the measured pressure, p_2, to a viscosity delay, solutions to the system of equations were carried out for the isothermal case, for a fluid having a constant pressure coefficient viscosity constant bulk modulus, and constant delay time (t_d). The viscosity functions thus become

$$F(T) = 1$$
$$G_e\,(p) = e^{\alpha p}$$

Also, a sinusoidal input was used as in the previous parametric studies.

Under these conditions non-dimensionalization shows $\tilde{p}_2(\tau)$ to be a function of four parameters. These are the parameters β and $\tilde{\alpha}$ used previously and two additional parameters τ_d and λ defined as

$$\tau_d = t_d/t_o \tag{43}$$

and

$$\lambda = \frac{\pi}{8}\frac{t_d a}{\mu_1}\left(\frac{R}{L}\right)^2 \tag{44}$$

The above two parameters are the effective delay parameter in the reservoir 1 (τ_d) and the delay parameter in the capillary (λ). The ratio of the two parameters

$$\frac{\tau_d}{\lambda} = \frac{8}{\pi}\frac{\mu_1}{a t_o}\left(\frac{L}{R}\right)^2$$

for a typical case corresponding to a pressure amplitude of a = 20 ksi, a capillary length of L = 0.3 inch, a radius of R = 2 mils, a duration time of t_o = 3 milliseconds and a viscosity of μ_1 = 25 cp is calculated to be 3.5×10^{-3}. The fact that this ratio is extremely small compared with the duration time of the pressure pulse; hence, for the parameter ranges of current interest, one of two extreme cases can be expected to occur. These are:

1. The delay in the capillary is of the order one or less, hence, there is no appreciable delay effect in the reservoir ($\tau_d \rightarrow 0$).

2. There is appreciable delay in the reservoir, hence, complete delay occurs in the capillary (the fluid viscosity in the capillary thereby being equal to the inlet viscosity) which would correspond to $\lambda \rightarrow \infty$.

Cases 1 and 2 are shown for typical values of β and $\tilde{\alpha}$ in Figures 29 and 30 respectively. It can be seen that in either case there will be considerable sensitivity to the delay parameters.

In general, delay times are expected to be small for the fluids, pressures and temperatures presently under consideration in comparison with the pulse time, t_o . Case 1 is thus anticipated to prevail with no significant delay effects in reservoir 1 and with delay effects in the capillary governed by the magnitude of the parameter λ.

The dwell time of a particle of fluid in the capillary can be regulated by regulating the length of the capillary as evidenced by the $(R/L)^2$ dependence of λ.

VISCOMETRIC ANALYSIS OF TEST DATA FOR A MIL-L-7808 FLUID

A summary of pertinent data for twelve different sets of pressure measurements for a MIL-L-7808 fluid is shown in the first four columns of Table 1. The first column of Table 1 contains the run number; the second column contains the amplitude of the inlet pressure, a, in thousands of psi; the third column contains the measured duration time, t_o, in milliseconds; and the fourth column contains the amplitude of the pressure in the discharge reservoir p_{2max}, in thousands of psi.

The pressure pulses, $p_1(t)$, were very nearly sinusoidal; hence, the amplitudes were sufficient for describing the entire curve along with the period, t_o. The remaining columns of Table 1 represent predictions of the peak pressure in reservoir 2, p_{2max}, on the basis of various viscometric assumptions. In all cases the bulk modulus of the fluid, which is an important property in determining p_2, was obtained from measurements provided in Reference (2) for MIL-L-7808 fluid at 70°F. The bulk modulus was fit in the zero to 50,000 psi region with a third order polynomial given below.

$$k = 2.739 \times 10^5 + 1.827p + 7.996 \times 10^{-5}p^2 - 7.615 \times 10^{-10}p^3$$

where p denotes the pressure in psi and k denotes the bulk modulus in psi.

Column five of Table 1 shows values of p_{2max} that would be predicted if the viscosity of the fluid were constant and equal to the measured value at 70°F of 23 centipoise. It is seen in all cases that when the viscosity is assumed to be constant at this value, the predicted values of p_{2max} are consistently lower than the measured values. This result was somewhat surprising at the outset since it is well known that the viscosity of a fluid increases with pressure and such increases in viscosity should result in more capillary resistance and still lower values of p_{2max}. Hence, the results shown in column 5 indicate that if isothermal operation were occurring, the fluid would have to have a negative pressure coefficient of viscosity which is totally unreasonable.

The above results suggested that thermal effects could indeed be influencing the results. The viscosity of a MIL-L-7808 oil was measured as a function of temperature over an interval of between 60°F and 300°F. The resultant (Fig. 31) viscosity-temperature curve was approximated with the viscosity index type formula given below.

$$\mu_e = \exp\{\exp[-3.705\ln(T + 460) + 24.39]\} - 0.87, \qquad p = 14.7$$

where the units for μ_e in the above expression are cp and T is in °F.

The above expression is accurate within the range of experimental accuracy of 1%. The next set of computations were carried out using the above viscosity temperature expressions, but still assuming no sensitivity to pressure. The results

TABLE 1 PRESSURE-PULSE SUMMARY DATA FOR MIL-L-7808 WITH CALCULATED PRESSURE-VISCOSITY COEFFICIENTS

Run Number	Pressure Trace Measurements			Calculated Information		
	Pressure Amplitude a (kpsi)	t_o (ms)	$p_{2\ max}$ (kpsi)	$p_{2\ max}$ Isoviscous $\alpha = 0$ (kpsi)	$p_{2\ max}$ Temperature Sensitive Viscosity $\alpha = 0$ (kpsi)	Pressure-Viscosity Coefficient, α From Measured $p_{2\ max}$ $(psi)^{-1}$
28	3.70	2.64	.690	.629	.741	$.50 \times 10^{-4}$
26	6.00	2.37	1.10	.929	1.21	$.50 \times 10^{-4}$
25	6.20	2.70	1.30	1.07	1.40	$.47 \times 10^{-4}$
29	7.00	2.35	1.30	1.07	1.46	$.50 \times 10^{-4}$
31	7.00	2.45	1.32	1.11	1.51	$.57 \times 10^{-4}$
30	7.54	2.40	1.37	1.18	1.63	$.74 \times 10^{-4}$
32	10.4	2.40	1.97	1.63	2.51	$.76 \times 10^{-4}$
41	11.25	7.20	4.60	4.27	5.71	$.70 \times 10^{-4}$
39	13.0	4.10	3.80	3.22	4.97	$.73 \times 10^{-4}$
35	13.7	4.40	4.60	3.59	5.57	$.49 \times 10^{-4}$
40	14.75	4.20	4.95	3.73	5.99	$.47 \times 10^{-4}$
33	17.0	4.00	4.95	4.14	7.08	$.75 \times 10^{-4}$
					Mean α =	$.60 \times 10^{-4}$
					α Mean Deviation ±	$.114 \times 10^{-4}$

Test Capillary C - Geometry Factor, 1.418×10^{-9}

are shown in column 6 of Table 1. Here in all cases the predicted pressure is substantially lower than the measured pressure, indicating that the true viscosity characteristics are somewhat higher than those assuming a zero pressure coefficient of viscosity. These results are somewhat more reasonable and considerably more encouraging.

The final step in the analysis of the data shown in Table 1 was to assume an exponential pressure dependence on viscosity accompanied by the temperature dependence described above and to find the value of the pressure coefficient of viscosity, α, for which the predicted and measured values of p_{2max} were identical. Values of α so obtained which were assumed independent of temperature, are shown in the seventh column of Table 1. The values range from $.47 \times 10^{-4}$ to $.75 \times 10^{-4}$ in ^{2}/lb with a mean value of $.60 \times 10^{-4}$ in ^{2}/lb and a mean deviation of 0.114×10^{-4} in ^{2}/lb. Values recorded in Reference (2) for a different batch of a similar fluid ranged from 10^{-4} in ^{2}/lb at 68°F to $.52 \times 10^{-4}$ in ^{2}/lb at 210°F, approximately. Hence, values of the pressure coefficient of viscosity extracted from pulse measurements appear to lie within the range of those obtained from previously reported data.

The above results indicate that the pulse viscometer appears to be a simple means for extracting pressure coefficients of viscosity. However, it is also seen that using reasonable values of pressure coefficients of viscosity the pulse data can be fit independently of any time delay phenomena and as such does not provide in itself a means for separating time effects from viscosity-pressure effects. In order to alleviate this difficulty, the dual capillary viscometer was constructed having two capillaries of different lengths. The different lengths result in significantly different residence times of a particle of fluid within the capillary and should provide relatively different delay behavior. This dual capillary viscometer arrangement with two secondary chambers (as shown schematically in Figure 32) which were connected by separate capillary tubes to the primary pressure chamber. The chamber volumes and capillaries were sized such that the geometry factor for both secondary chambers were nearly equal to one another. In this case, the diameter of each capillary was the same. The system provides two simultaneous pressure measurements. The first of these is the inlet pressure, $p_1(t)$, as a function of time which is the same for both capillaries. The second measurement is a pressure difference or the difference in values of $p_2(t)$ between the two exit reservoirs referred to as $\Delta p_2(t)$.

In order to confine our attention to a situation providing as strong a time delay as possible, our efforts were concentrated on one pulse obtained with the use of a drop table at the pressure amplitude of the order of 20,000 psi. The pulse data as photographed on the oscilloscope is shown in Figure 33. In this case it is clearly seen that the input pulse is not sinusoidal, hence it was necessary to extract the data digitally from the photographs and feed in the input pulse, $p_1(t)$, into the computer to calculate the pressure difference $\Delta p_2(t)$. The two capillaries differ by approximately a factor of three in length and values of $\Delta p_2(t)$ correspond to values of $p_2(t)$ obtained from the short capillary subtracted from values of $p_2(t)$ obtained from the long capillary. The measured peak pressure difference, Δp_{2max}, is approximately 2800 psi.

The first step in the analysis of this data was to compute the analytical

C

values of the pressure difference, $\Delta p_2(t)$ assuming no time delay, but including variations of bulk modulus with pressure and variations of viscosity with pressure and temperature. The results of these predicted measurements are shown in Figure 34. Measured and predicted values of Δp_{2max} are plotted as functions of the pressure coefficient of viscosity. It can be seen that variations in the pressure coefficient of viscosity within a reasonable range cannot nearly account for differences between predicted and measured values of Δp_{2max}.

At this stage, the full computer analysis described in the previous section was run with the inclusion of viscosity pressure, and temperature effects along with viscosity-time effects. The two triangular points shown in Figure 34 correspond to calculated values of Δp assuming a constant delay time of t_d = 2 microseconds. It is seen here that the inclusion of viscosity delay time goes a long way toward reconciling predicted and measured values of Δp_{2max}. As calculations are costly here, no attempt was made to fully bracket the measurements of Δp_{2max} by varying the delay time.

As a result of the temperature rises in the capillary, it is possible that the viscosity can fall low enough to induce local turbulence. Such turbulence, if it did occur, could provide results in the same direction as those produced by short-time effects. It is doubtful, however, that turbulence could develop in the short times (less than 3 milliseconds) that the lubricant is subjected to the high pressure difference. The probability of turbulence would be greatly reduced with the use of smaller diameter capillaries and such experiments should be performed. The use of smaller diameter capillaries would also eliminate inertial effects which have not as yet been considered in the analysis but could become significant at higher Reynold numbers.

SUMMARY AND CONCLUSIONS

A pulse type capillary viscometer has been developed which appears to be capable of predicting pressure coefficients of viscosities with a simpler type of device than has heretofore been available. In addition, the apparatus offers attractive prospects with regard to extracting viscosity-time characteristics. Preliminary experiments with a MIL-L-7808 oil indicate a delay time to exist in the order of 2 microseconds which is a qualitative range of the viscosity delay or time effects observed in elastohydrodynamic rolling disc tractions.

There are, however, several problems associated with the test apparatus. Thermal effects are prevalent as a result of viscous heating in the capillary, however they are believed to be fairly analyzable. There is also a possibility of local turbulence occurring in some of the capillaries at some of the higher pressure differences.

On the basis of the above conclusions, it is recommended that further modifications be performed to insure that there is no turbulence in the apparatus and to attempt to reduce thermal effects. One such method for doing this would be to apply an over pressure to the apparatus so that viscous characteristics at higher pressures could be investigated without resorting to extreme pressure differences. This would both reduce the thermal problem, inertial effects, and the tendency for turbulence. The use of an over pressure together with the ability to subject the apparatus to different ambient temperatures would provide a versatile viscometer for extracting more conventional viscosity-pressure characteristics under long times in a simpler manner than has been heretofore possible along with providing the ability to extract short time viscosity characteristics.

REFERENCES

1. Klaus, E.E., Johnson, R.H., and Fresco, G.P., "Development of a Precision Capillary Type Pressure Viscosimeter," Trans. ASLE, Vol. 9, 1966, p. 113.

2. Wilson, D.R., Bossert, A.J., "Exploratory Development on Advanced Fluids and Lubricants in Extreme Environments by a Mechanical Characterization," Tech. Report AFML-TR-70-32, WPAFB, Ohio, 1971.

APPENDIX 1

EQUIPMENT LIST

One Harwood Engineering pressure intensifier Model E-1986

Two Vishay Intertechnology Incorporated strain gage bridges and amplifiers Model BAM-1

One Tektronix Model 502A dual beam oscilloscope

One Weston digital voltmeter Model 1420

Micro-measurements foil gages #VM-SS-125CH-048

Charles T. Gamble Incorporated subminiature resistors, manganin #200200AL, non-inductive wound

One Spectra Physics helium-neon laser Model 132

One Mechanical Technology Incorporated Fotonic sensor Model KD-38

Machined Items per ten MTI drawings Series 264

APPENDIX 2

LUBRICANT PROPERTIES

Physical Property	MIL-L-7808 Humble Oil #2389	Polyphenyl Ether Monsanto OS-124	MIL-L-23699A Mobile Jet II	Synthetic Hydrocarbon XRM 214B
Density (gm/ml)				
68°F	.9500	---	---	---
100°F	1.0007	1.19	.986	.824
210°F	.8940	1.14	.940	---
Viscosity (cps)	Temperature = 68°F	Temperature = 100°F	Temperature = 100°F	Temperature =100°F
Atmospheric	25	355 at 1 ATM	29	53
10 kpsi	78	661 at 2000 psig	91	---
20 kpsi	189	1225 at 4000 psig	333	---
30 kpsi	454	2495 at 8000 pisg	---	---
Bulk Modulus (psi)				
68°F	See Text for Formula	---	---	---
100°F		390,000	210,000	---
210°F		320,000	110,000 at 300°F	---
Temperature-Viscosity Coefficient $^{o}F^{-1}$	See Text	.046	---	---
Thermal Conductivity BTU/hr/ft/°F	.056	.056	.086	---
Specific Heat BTU/lb-°F	.5	.5	.447	.498
Pressure-Viscosity Coefficient in^2/lb	See Text	1.38×10^{-4}	---	---

NOMENCLATURE

A	Cross-section of piston	in^2
a	Input pulse amplitude	lb/in^2
c	Specific heat	$in\text{-}lb/lb_m/^oF$
E	Mechanical pulse energy	in-lb
F	Viscosity-temperature function	
f	Dimensionless pressure in reservoir 1	
G	Dimensionless viscosity-pressure function	
G_e	Dimensionless equilibrium viscosity-pressure function	
G_1	Value of G in reservoir 1	
$g(p)$	Dimensionless viscosity function	
g^*	Dimensionless viscosity function	
k	Bulk modulus	lb/in^2
L	Capillary length	in.
M	Mass of piston	$lb\text{-}sec^2/in$
p	Pressure	lb/in^2
p_1, p_2	Pressure reservoirs 1 and 2	lb/in^2
$\tilde{p}_2$	Dimensionless pressure in reservoir 2	
p_{2max}	Maximum value of p_2	
Q	Flow rate	in^3/sec
R	Radius of capillary	in.
r	Radial coordinate	in.
T	Temperature	^oF
T_o	Reference temperature	^oF
T_1	Temperature in reservoir 1	^oF
t	Time	sec.
t_d	Delay time constant	sec.
t_o	Pulse duration time	sec.
u	Flow velocity	in/sec
$\bar{u}$	Average flow velocity	in/sec
V_1, V_2	Volume reservoirs 1 and 2	in^3
z	Axial coordinate	in.

NOMENCLATURE (Continued)

α	Pressure coefficient of viscosity	in^2/lb
$\tilde{\alpha}$	Dimensionless pressure coefficient of viscosity αa	
β	Dimensionless flow parameter	
δ	Viscosity-temperature coefficient	$^oF^{-1}$
$\tilde{\delta}$	Dimensionless viscosity-temperature coefficient, $a\delta$	
Δp_2	Pressure difference between discharge reservoir	psi
Δp_{2max}	Maximum value of Δp_2	psi
λ	Dimensionless capillary delay parameter	
μ	Viscosity	$lb\text{-}sec/in^2$
μ_e	Equilibrium viscosity	$lb\text{-}sec/in^2$
μ_o	Reference viscosity at atmospheric pressure	$lb\text{-}sec/in^2$
μ_1	Viscosity in reservoir 1	$lb\text{-}sec/in^2$
ρ	Density	lb_m/in^3
ρ_o	Reference density	lb_m/in^3
τ	Dimensionless time, t/t_o	
τ_d	Dimensionless delay constant t_d/t_o	
τ_{max}	Dimensionless time at which $\tilde{p}_2$ is maximum	
Φ_L	Heat generation rate/unit length	lb-sec
Φ_v	Heat generation rate/unit volume	$lb/in^2/sec$
$\emptyset$	Dimensionless pressure function	

FIGURES

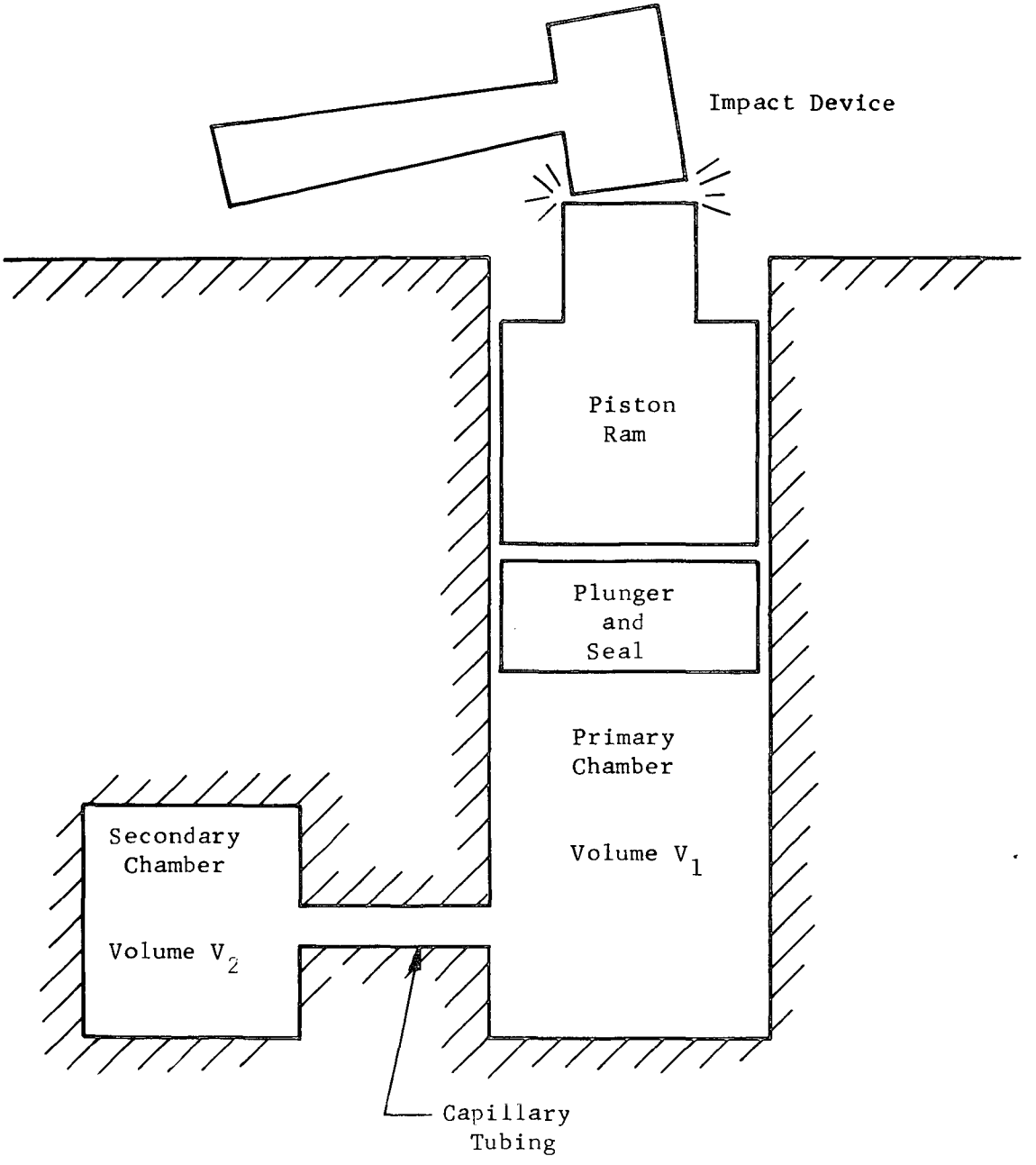

Fig. 1 Pulsed Viscometer Schematic

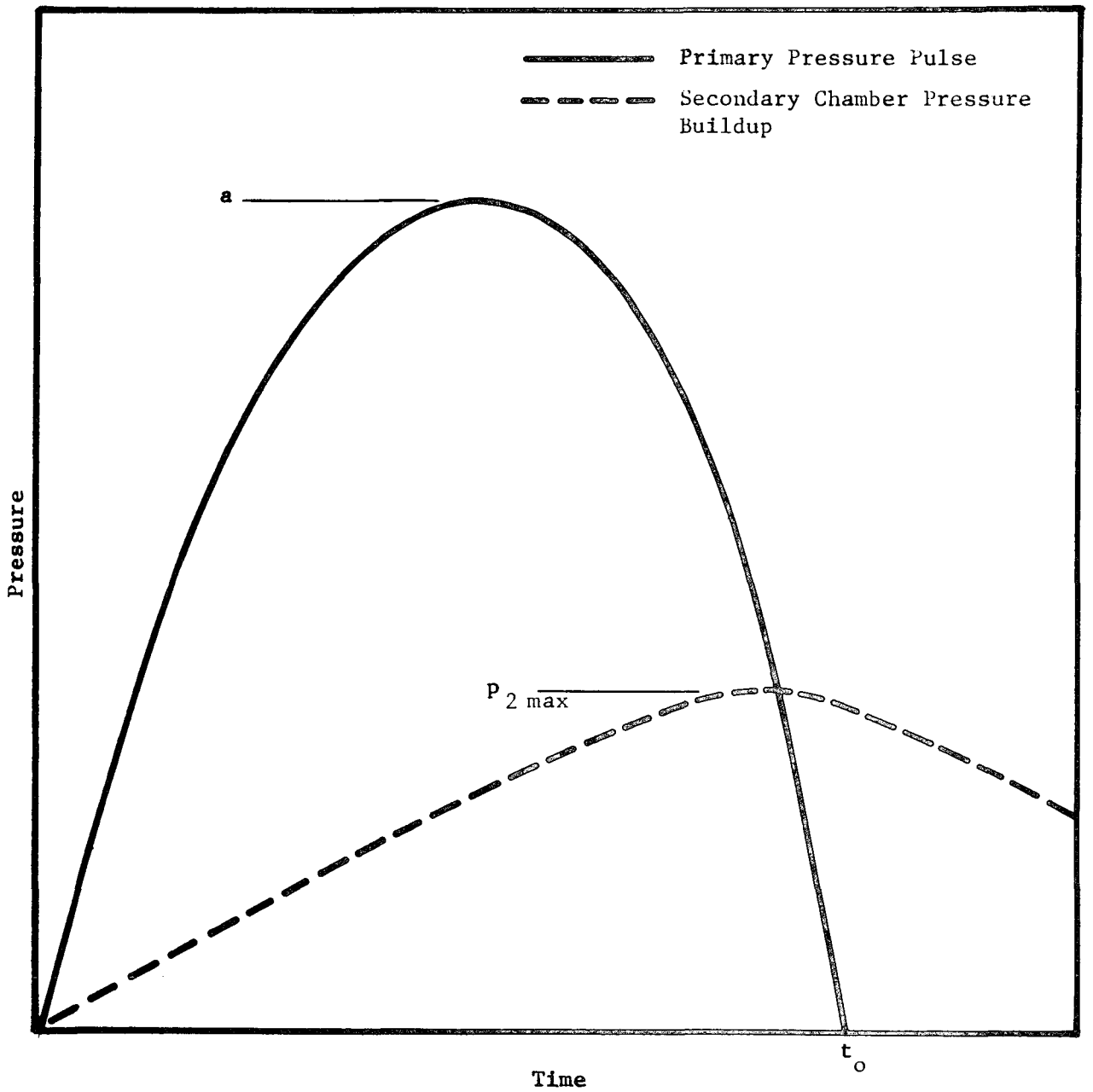

Fig. 2 Schematic of Measured Chamber Pressure Pulses

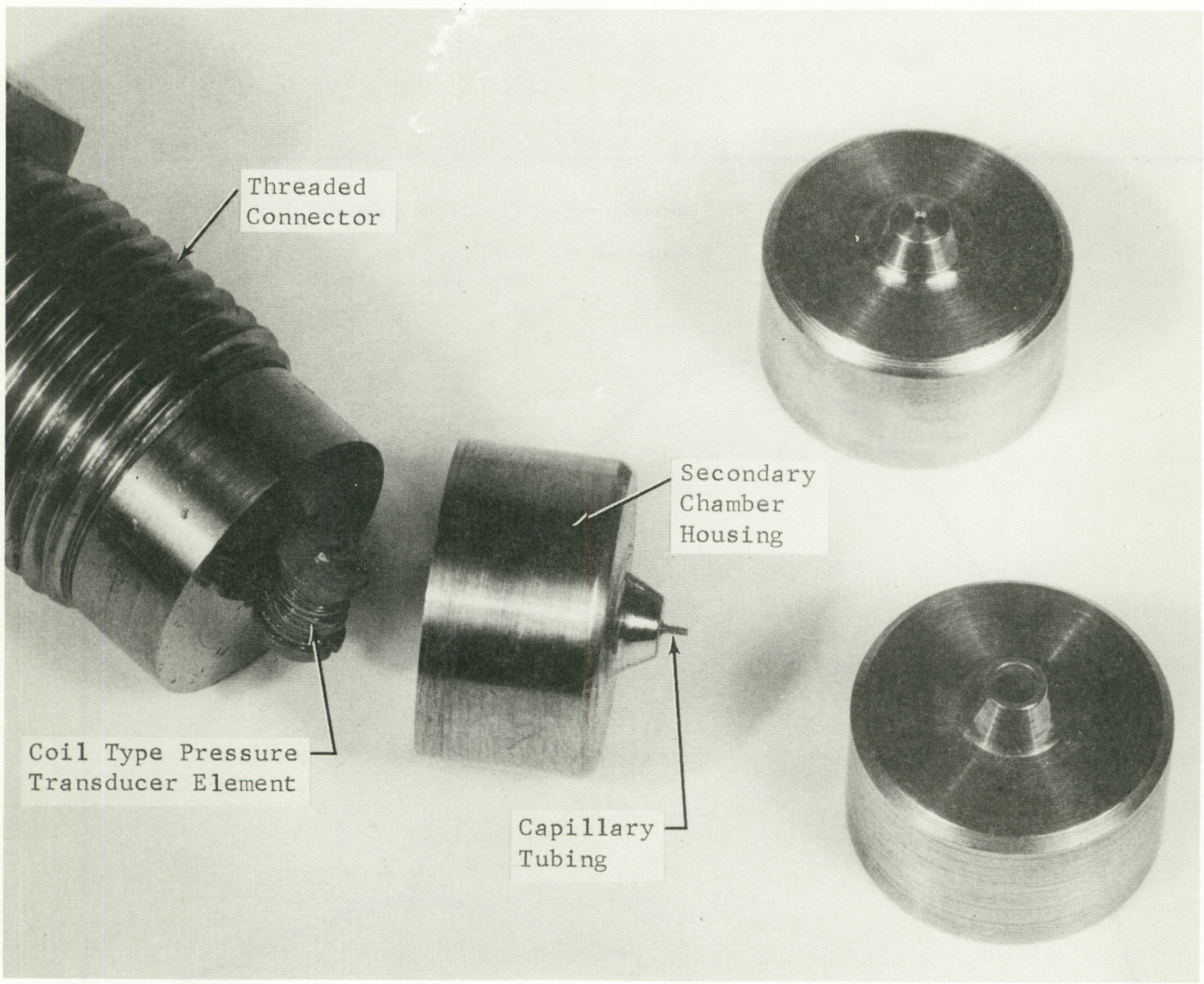

Fig. 3 Secondary Chamber Components Showing Capillary Tubing

MTI-13658

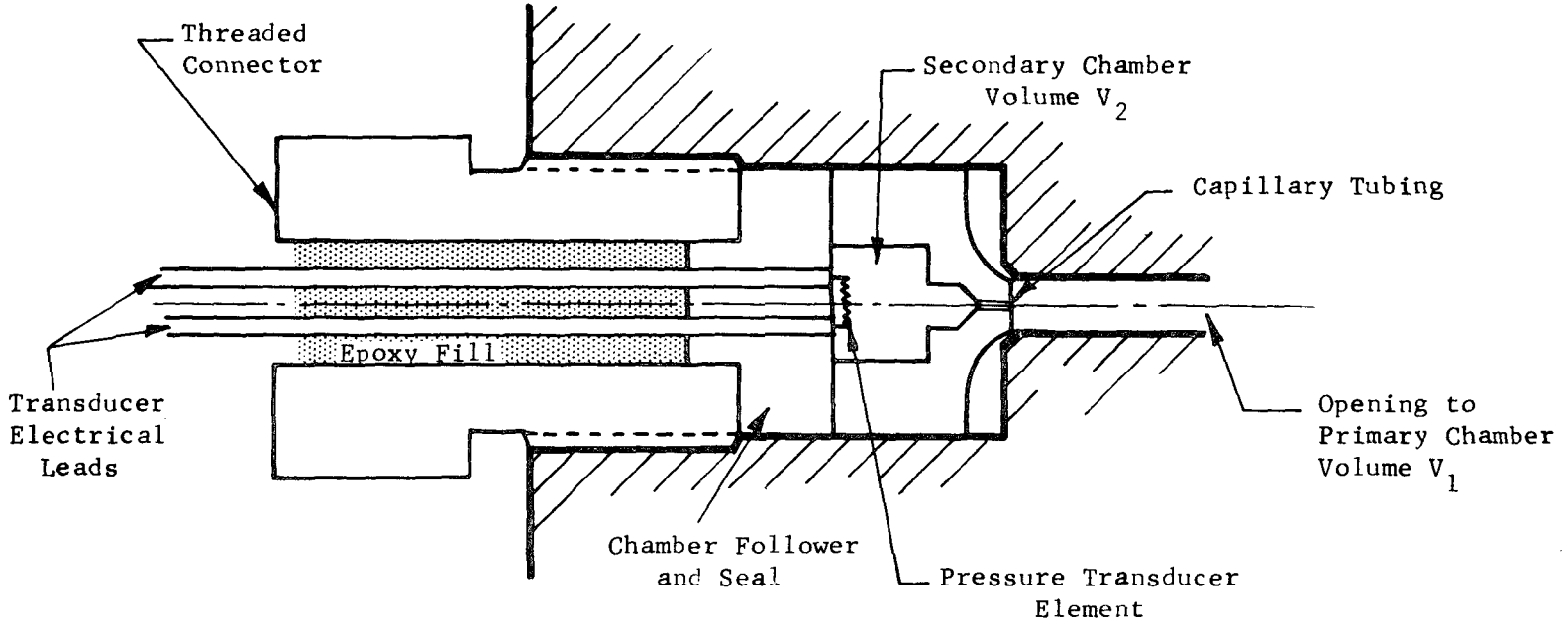

Fig. 4 Cross Sectional View of Typical Secondary Chamber V_2 and Feed Through Capillary Tubing

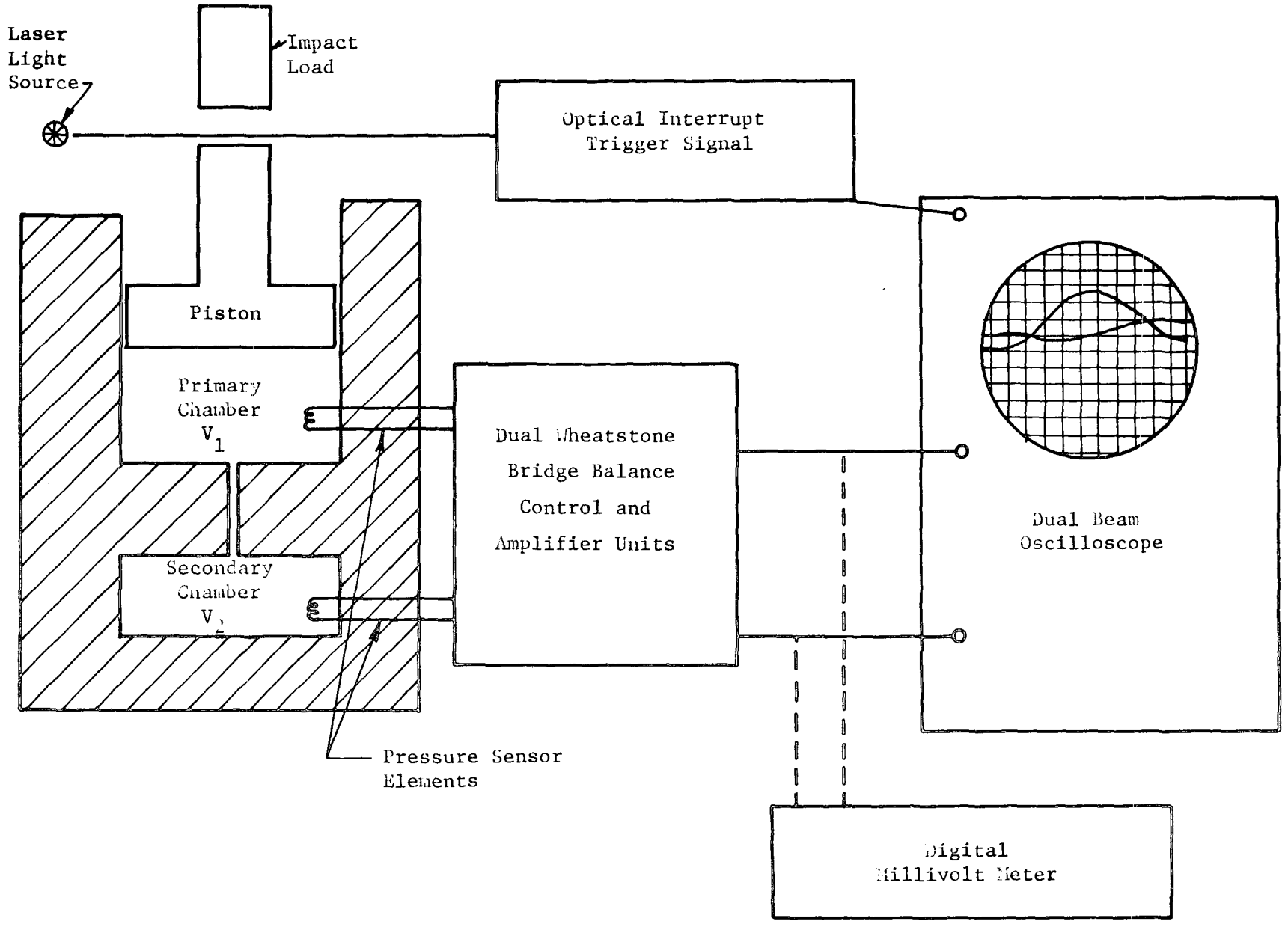

Fig. 5 Instrumentation Arrangement

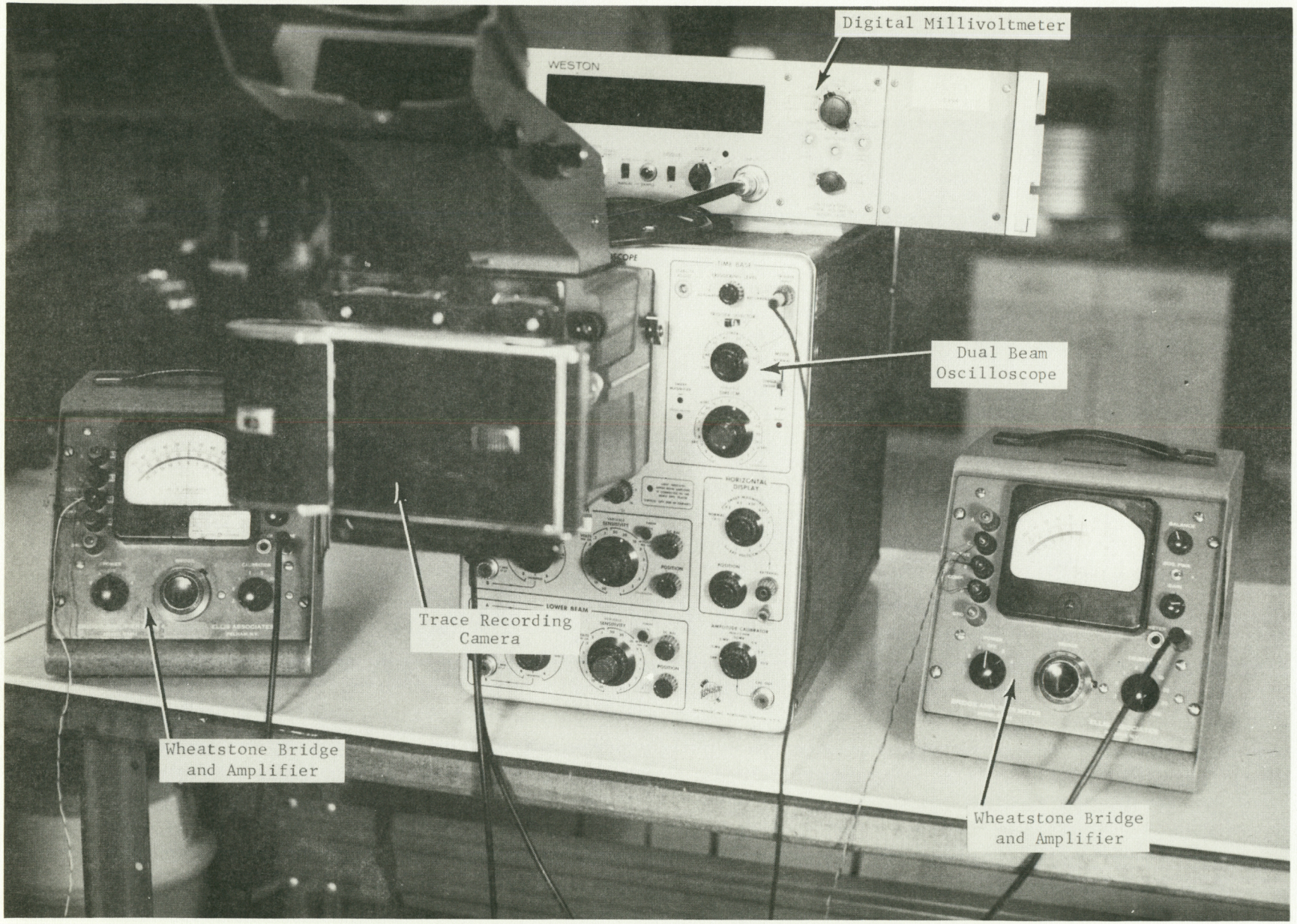

Fig. 6 Bridge and Oscilloscope Instrumentation

MTI-13659

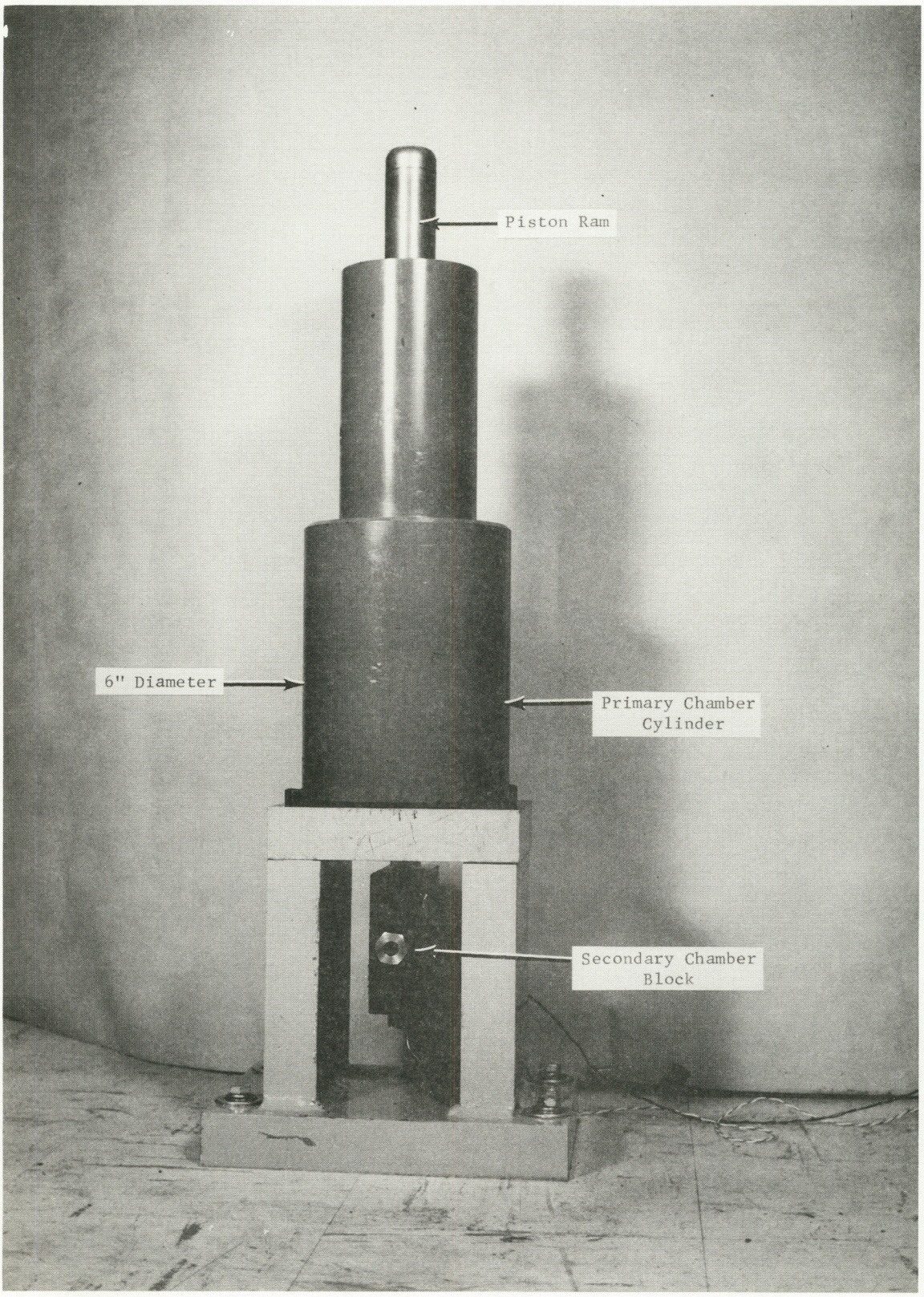

Fig. 7 High Pressure Chambers

Fig. 8 Pulsed Pressure Data

p_1 = 3,700 psi

p_2 = 690 psi

t_o = 2.65 milliseconds

Capillary: C

Lubricant: 7808

Run #28

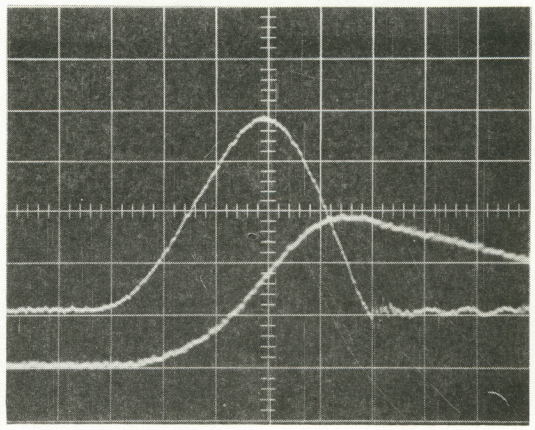

Fig. 9 Pulsed Pressure Data

p_1 = 7,000 psi

p_2 = 1,300 psi

t_o = 2.35 milliseconds

Capillary: C

Lubricant: 7808

Run #29

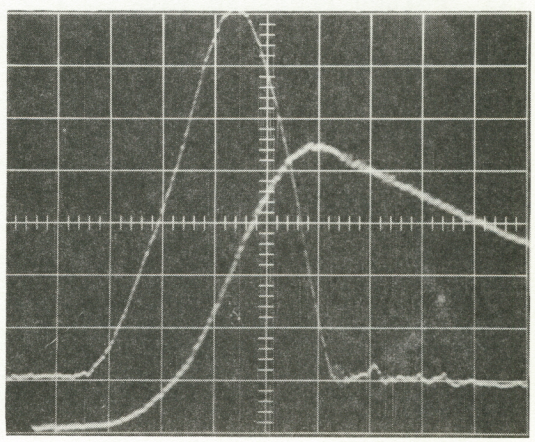

Fig. 10 Pulsed Pressure Data

p_1 = 10,400 psi

p_2 = 1,970 psi

t_o = 2.4 milliseconds

Capillary: C

Lubricant: 7808

Run #32

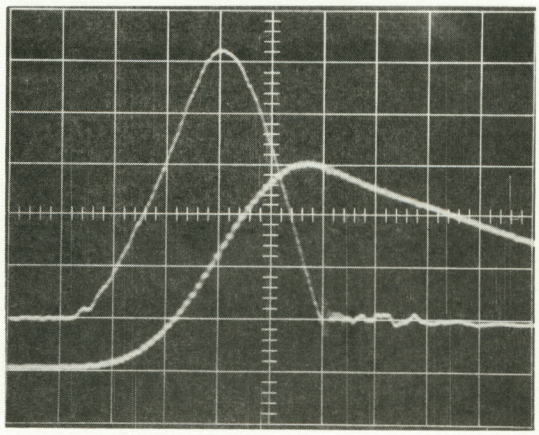

Fig. 11 Pulsed Pressure Data

p_1 = 14,750 psi

p_2 = 4,950 psi

t_o = 4.2 milliseconds

Capillary: C

Lubricant: 7808

Run #40

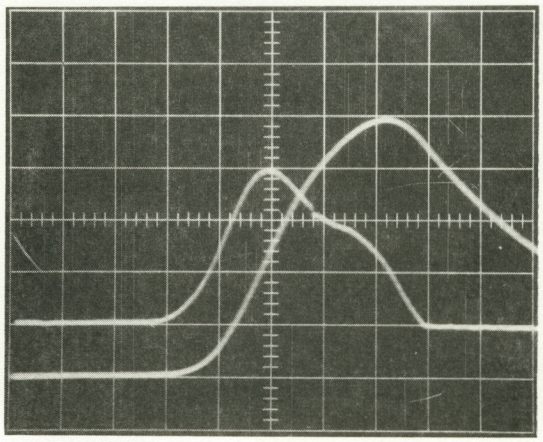

Fig. 12 Pulsed Pressure Data

p_1 = 7,600 psi

p_2 = 840 psi

t_o = 2.30 milliseconds

Capillary: C

Lubricant: Jet II

Run #58

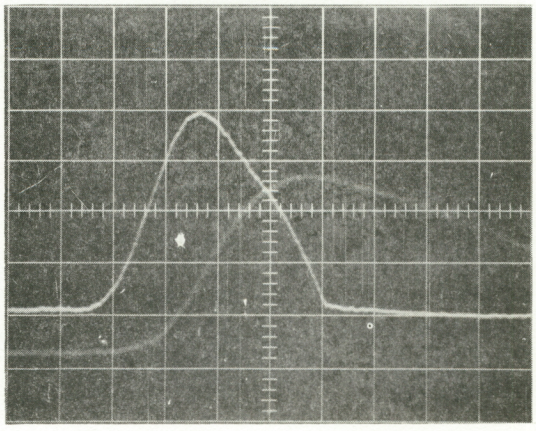

Fig. 13 Pulsed Pressure Data

p_1 = 10,000 psi

p_2 = 2,700 psi

t_o = 5.50 milliseconds

Capillary: C

Lubricant: Jet II

Run #66

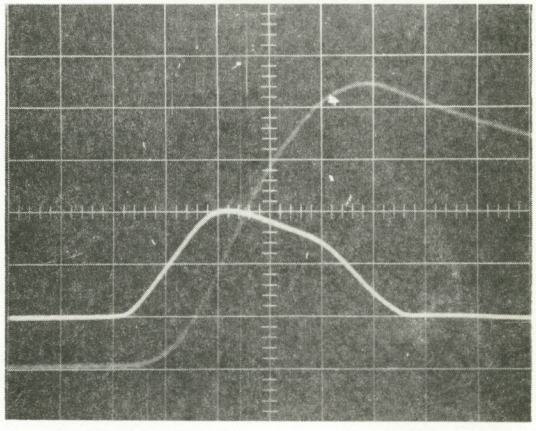

Fig. 14 Pulsed Pressure Data

p_1 = 18,700 psi

p_2 = 4,000 psi

t_o = 4.7 milliseconds

Capillary: C

Lubricant: Jet II

Run #67

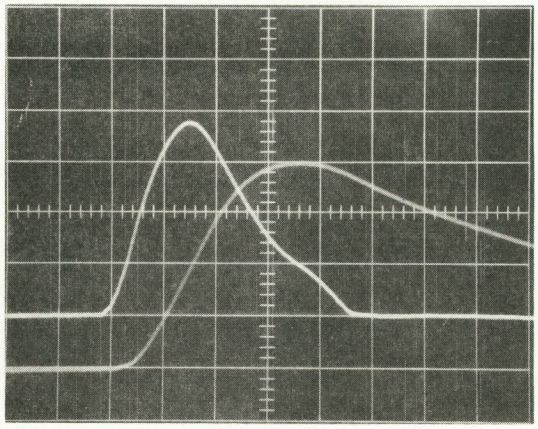

Fig. 15 Pulsed Pressure Data

p_1 = 31,000 psi

p_2 = 19,200 psi

t_o = 6.6 milliseconds

Capillary: E

Lubricant: Jet II

Run #84

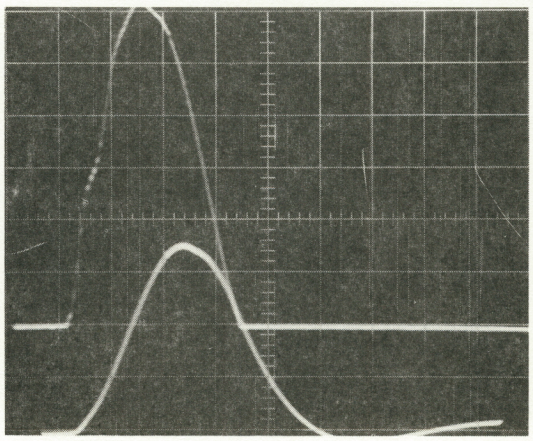

Fig. 16 Pulsed Pressure Data

p_1 = 8,400 psi

p_2 = 1,170 psi

t_o = 4.7 milliseconds

Capillary: E

Lubricant: XRM 214B

Run #95

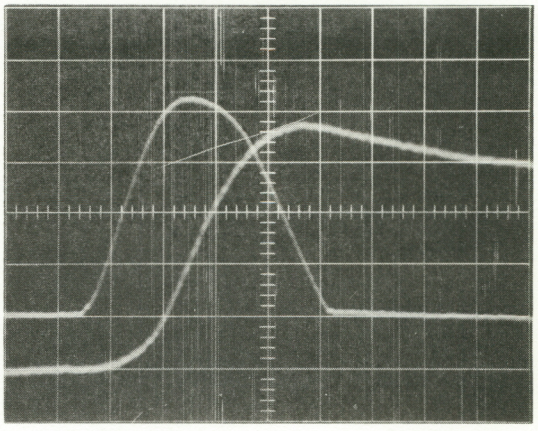

Fig. 17 Pulsed Pressure Data

p_1 = 9,200 psi

p_2 = 1,450 psi

t_o = 4.9 milliseconds

Capillary: E

Lubricant: XRM 214B

Run #90

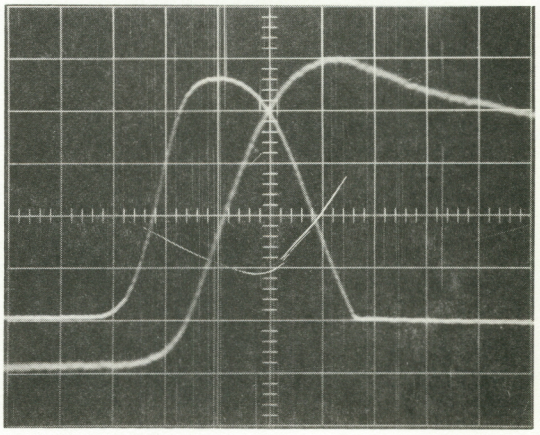

Fig. 18 Pulsed Pressure Data

p_1 = 22,200 psi

p_2 = 8,500 psi

t_o = 8.3 milliseconds

Capillary: E

Lubricant: XRM 214B

Run #100

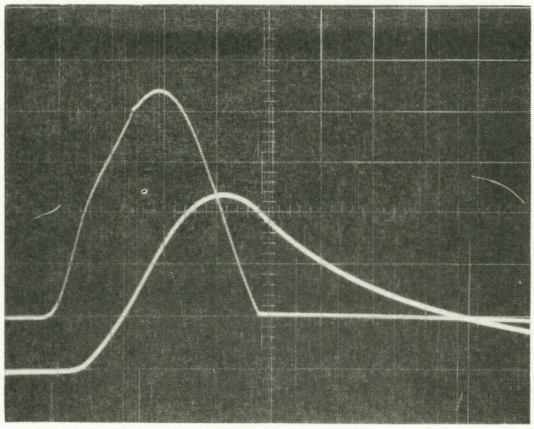

Fig. 19 Pulsed Pressure Data

p_1 = 27,000 psi

p_2 = 10,300 psi

t_o = 8.0 milliseconds

Capillary: E

Lubricant: XRM 214B

Run #101

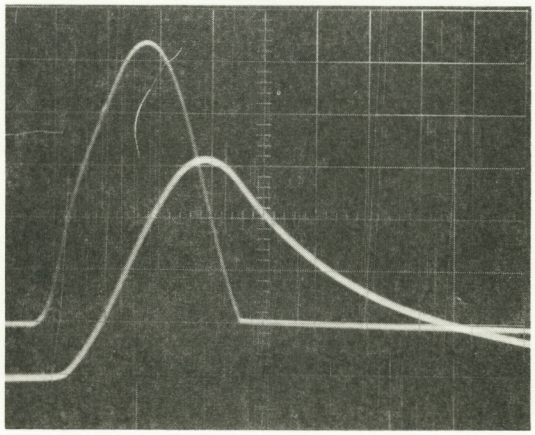

Fig. 20 Pulsed Pressure Data

p_1 = 9,300 psi

p_2 = 6,000 psi

t_o = 5.8 milliseconds

Capillary: B

Lubricant: Polyphenyl Ether

Run #135

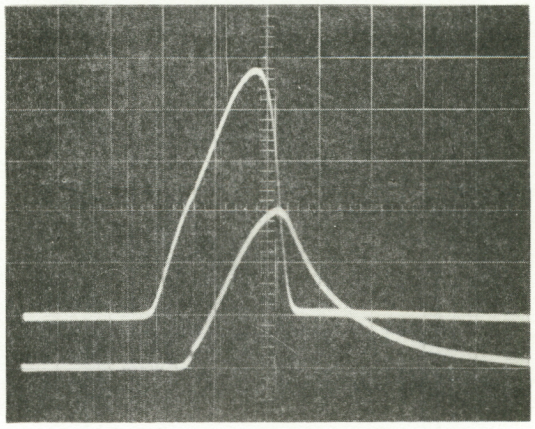

Fig. 21 Pulsed Pressure Data

p_1 = 12,200 psi

p_2 = 8,800 psi

t_o = 5.4 milliseconds

Capillary: B

Lubricant: Polyphenyl Ether

Run #119

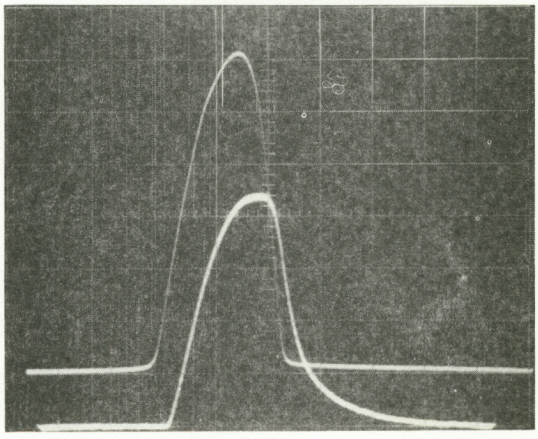

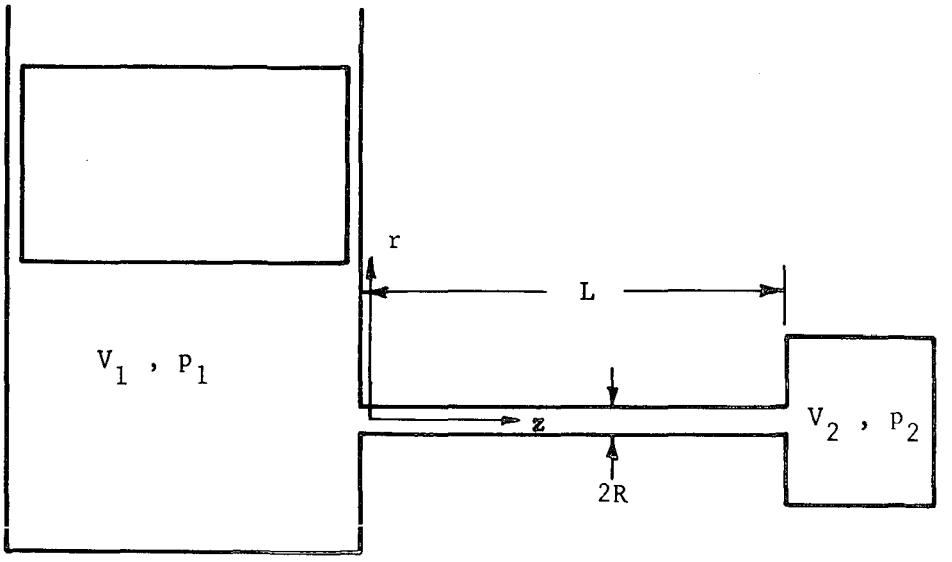

Fig. 22 Schematic of Geometry Used in Development of Analyses

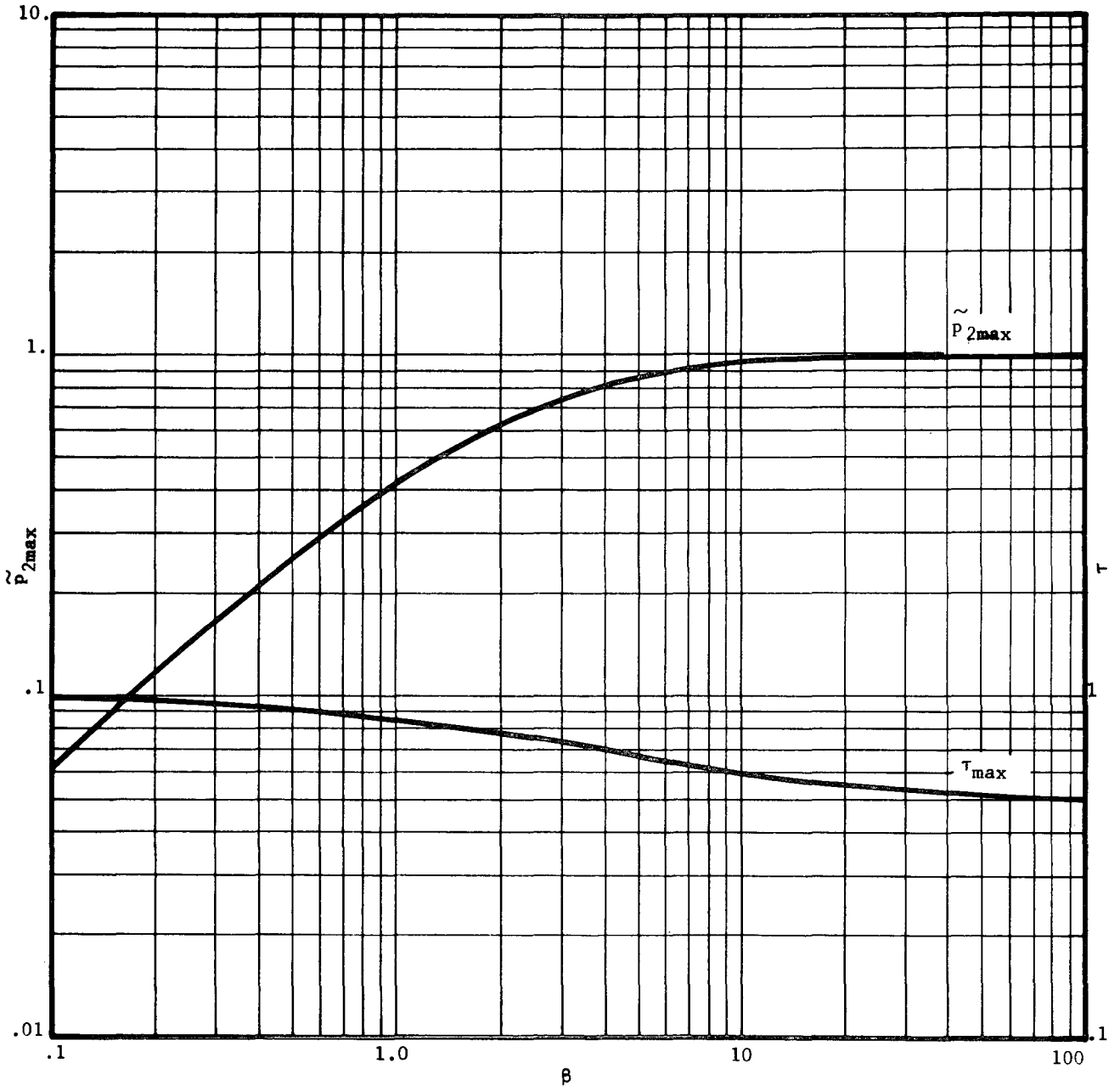

Fig. 23 The Variation of Peak Pressure and Pulse Time for an Isoviscous Fluid

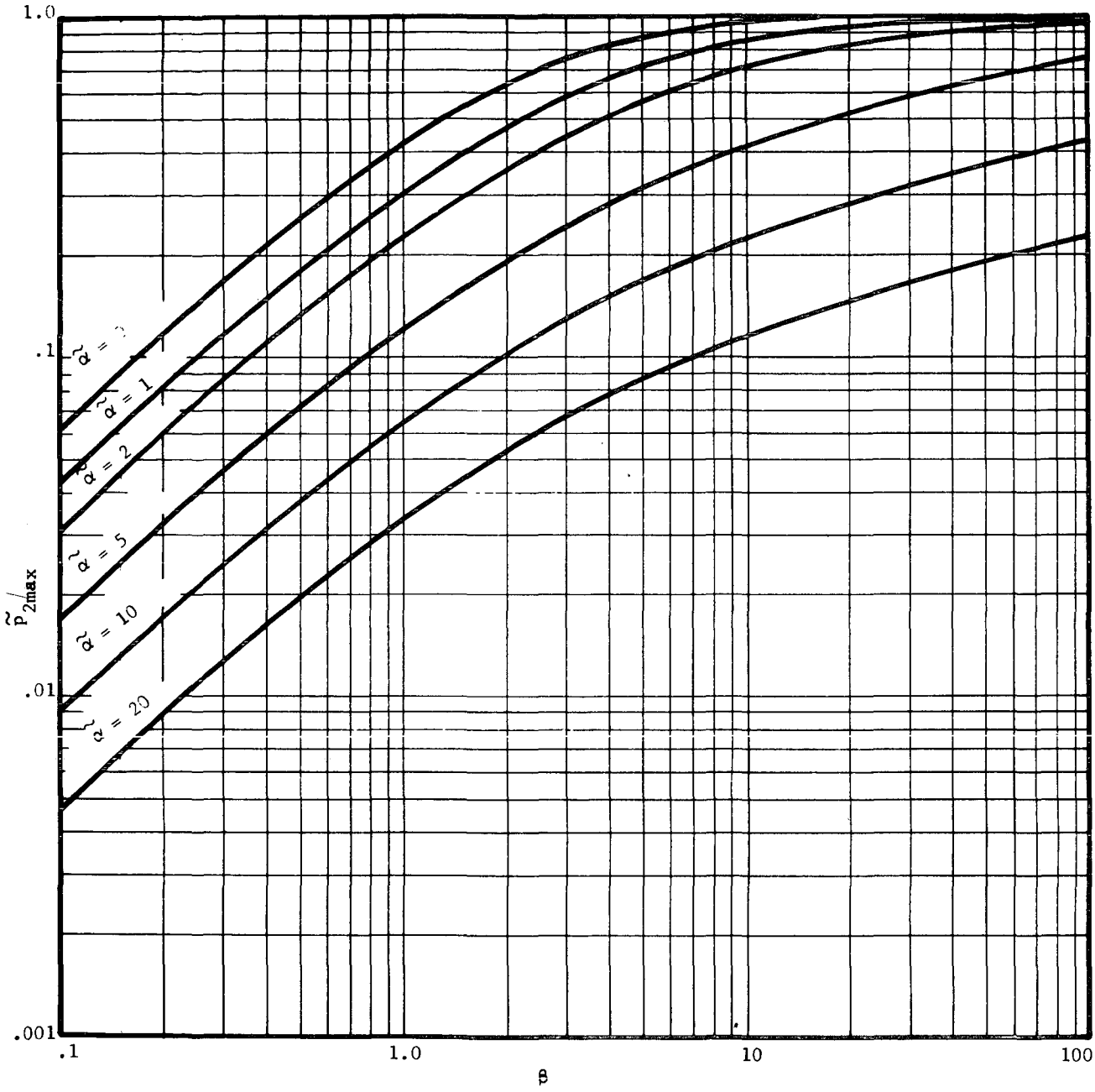

Fig. 24 The Effect of Pressure Coefficient of Viscosity on Predicted Pulse Measurements

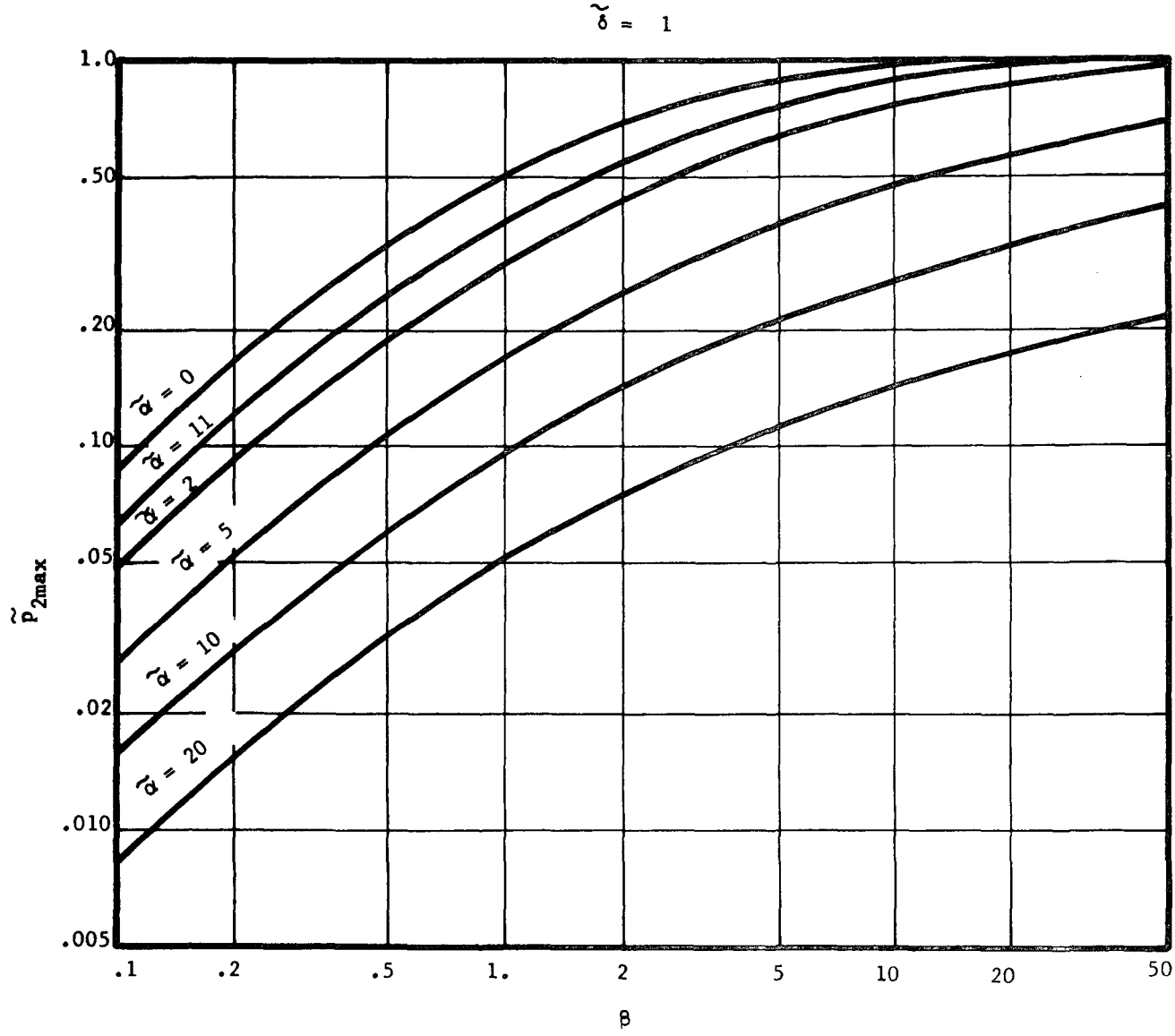

Fig. 25 The Effect of Viscosity Pressure and Temperature Coefficients on Predicted Pulse Measurements $\tilde{\delta}$ = 1

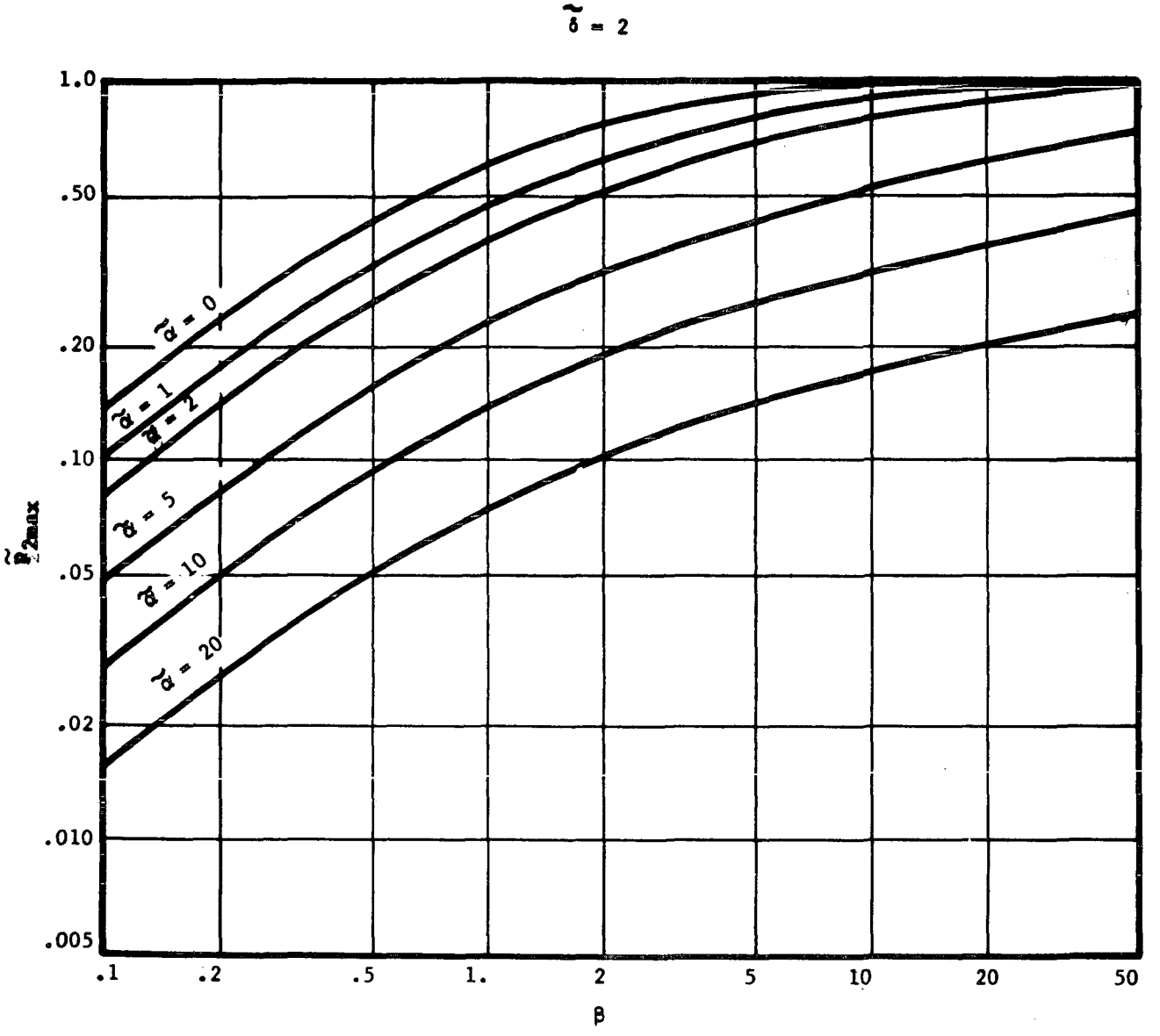

Fig. 26 The Effect of Viscosity Pressure and Temperature Coefficients on Predicted Pulse Measurements $\tilde{\delta} = 2$

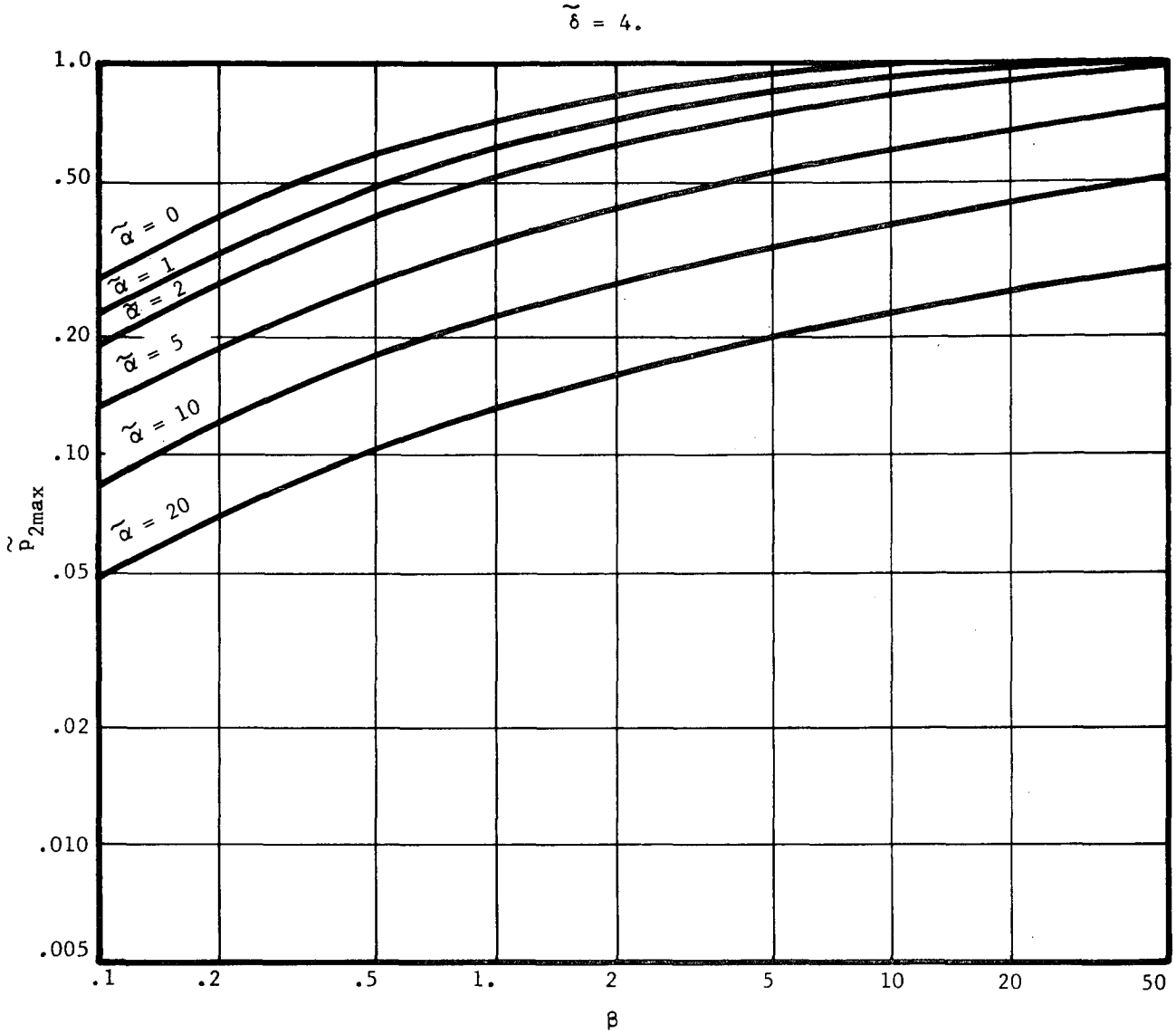

Fig. 27 The Effect of Viscosity Pressure and Temperature Coefficients on Predicted Pulse Measurements $\tilde{\delta} = 4$

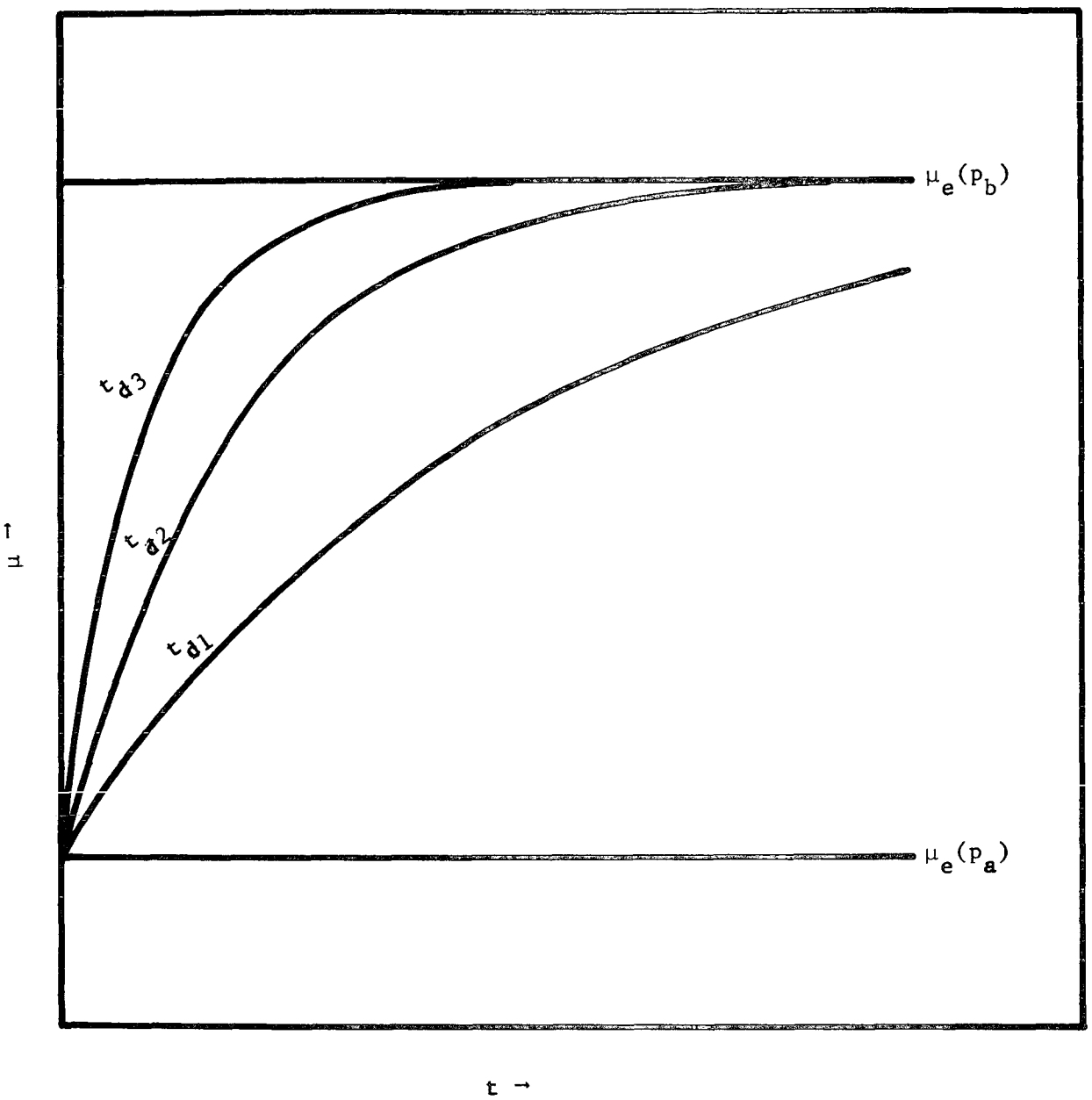

Fig. 28 Schematic of Viscosity Response to a Step Jump in Pressure ($t_{d1} > t_{d2} > t_{d3}$)

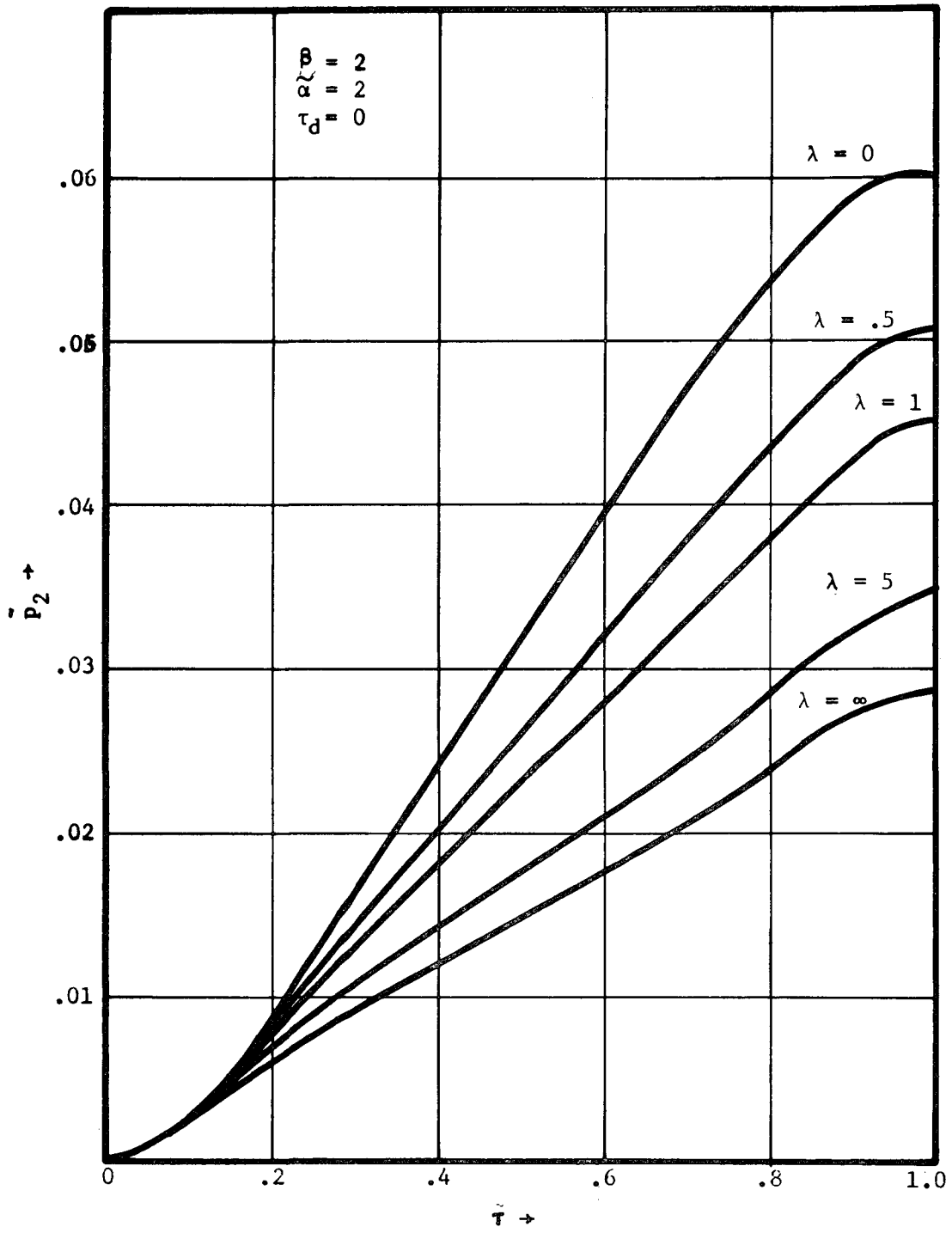

Fig. 29 Dimensionless Pressure-Time Curves for $\tau \rightarrow 0$

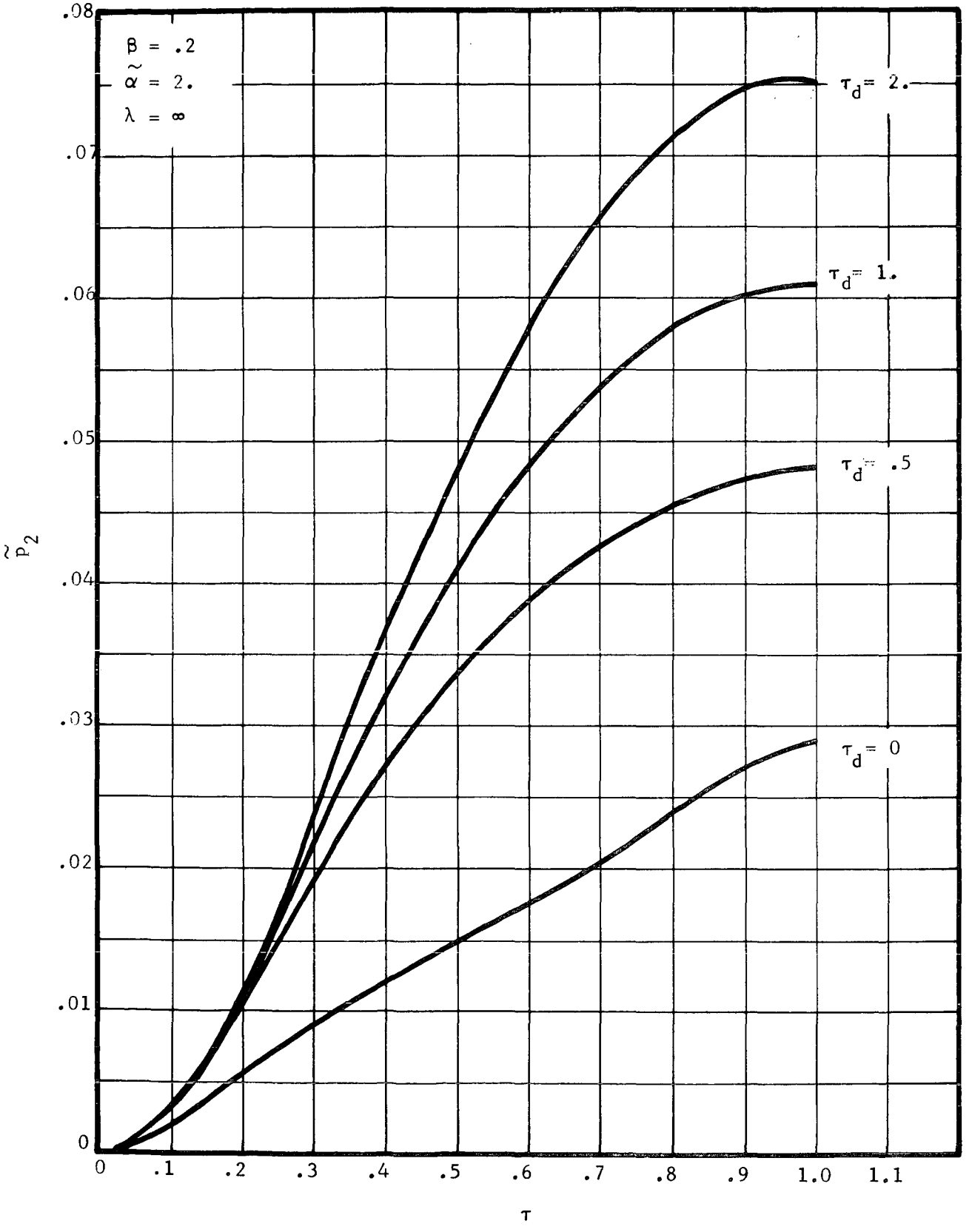

Fig. 30 Dimensionless Pressure-Time Curves for $\lambda \to \infty$

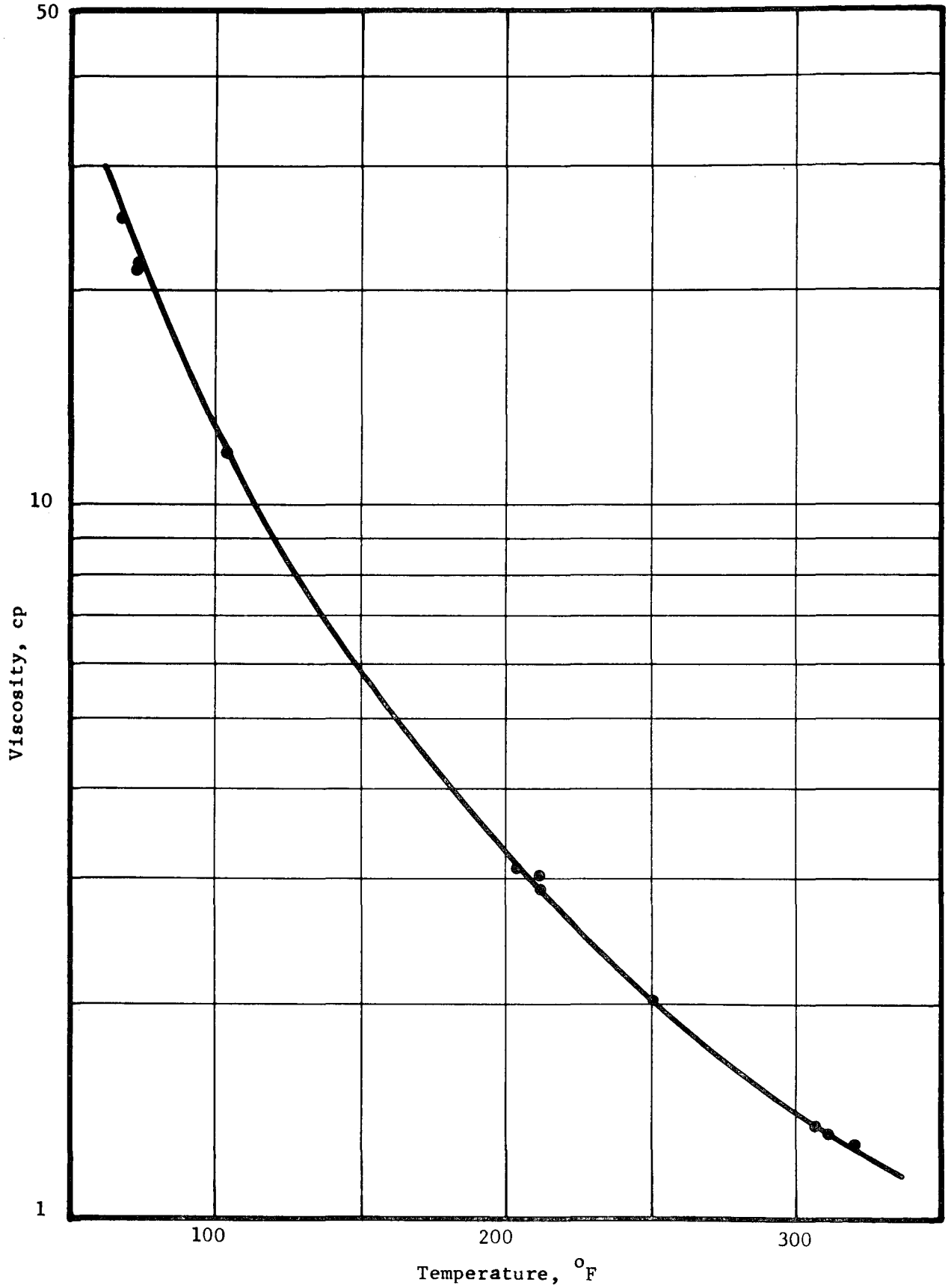

Fig. 31 Viscosity-Temperature Data at Atmospheric Pressure

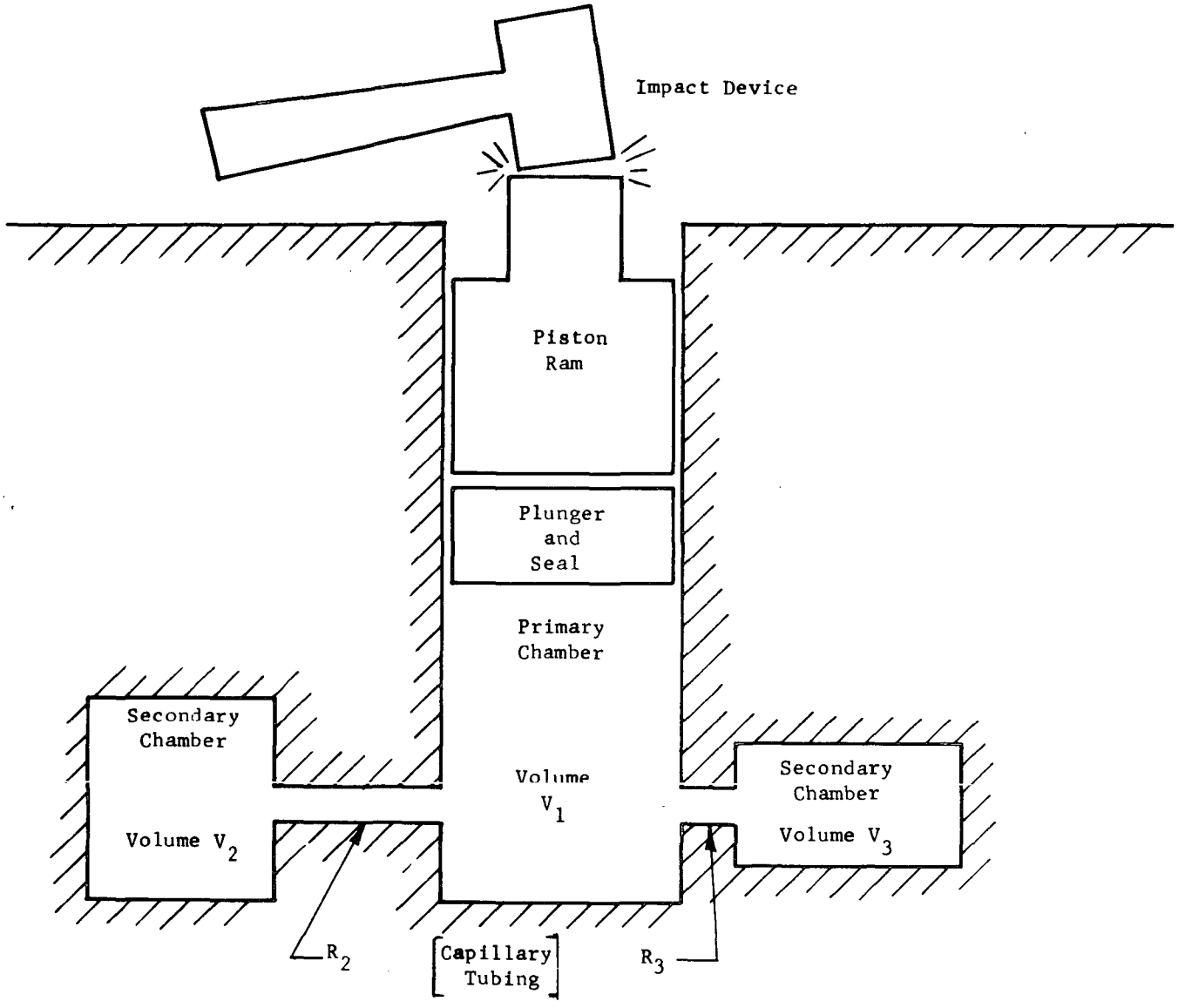

- Left capillary longer than right capillary
- $V_1 >> (V_2 + V)$

Fig. 32 Differential Pulsed Viscometer Schematic

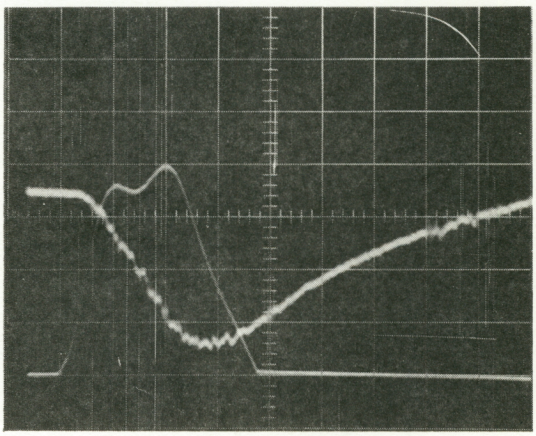

Fig. 33 Pulsed Pressure Data

p_1 = 20,000 psi

p_2-p_3 = 2,800 psi

t_o = 3.8 milliseconds

Capillaries: D & E

Run #113

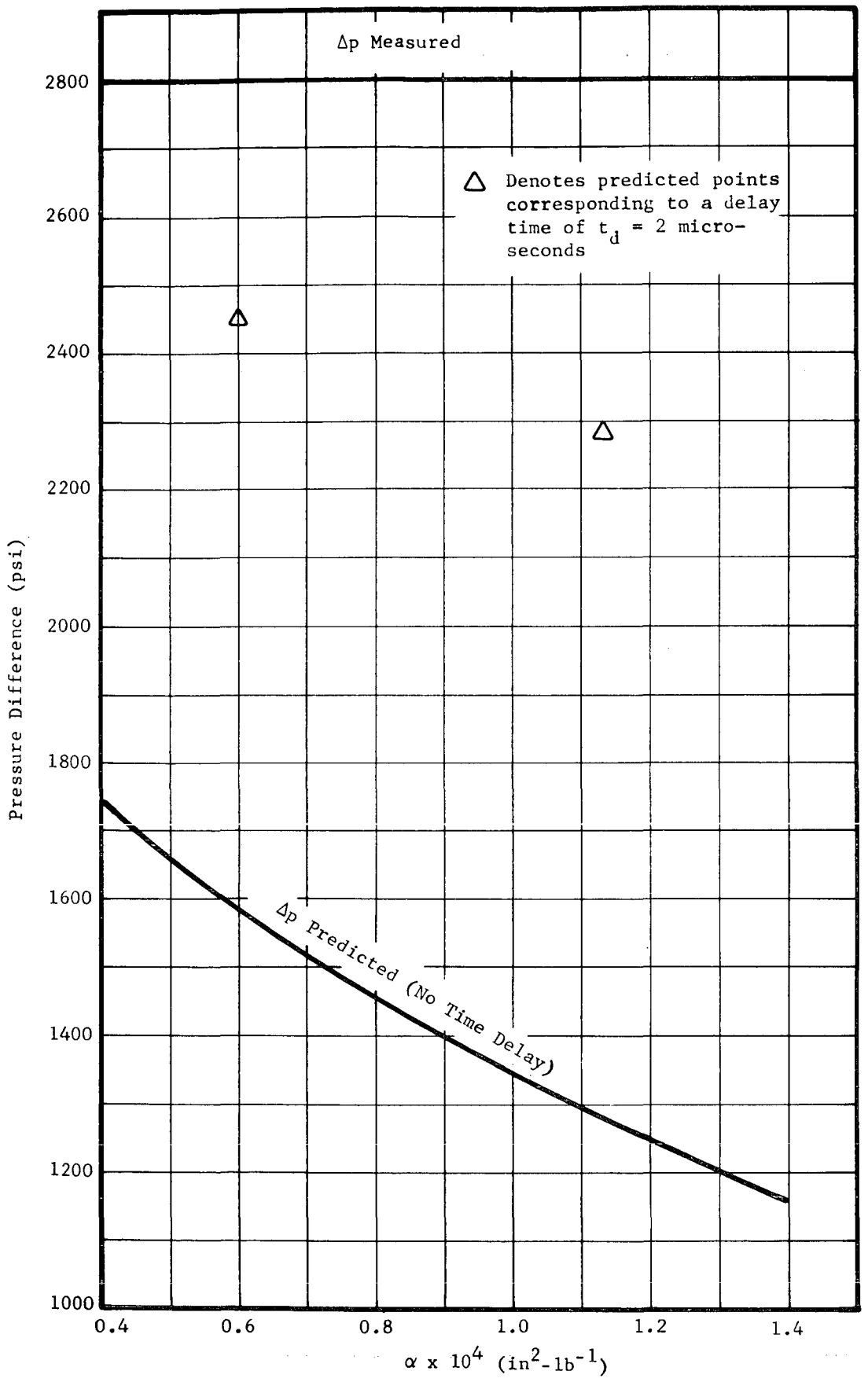

Fig. 34 Comparison Between Predicted and Measured Pressure Differences

DISTRIBUTION

NASA Lewis Research Center
21000 Brookpark Road
Cleveland, Ohio 44135

William J. Anderson
Project Manager
Mail Stop 23-2 (10 + reproducible)

E. E. Bisson
Mail Stop 5-3 (1)

W. J. Anderson
Mail Stop 23-2 (1)

R. L. Johnson
Mail Stop 23-2 (1)

G. Mervin Ault
Mail Stop 3-13 (1)

J. E. Dilley
Mail Stop 500-309 (1)

C. H. Voit
Mail Stop 5-3 (1)

Report Control Office
Mail Stop 5-5 (1)

Library
Mail Stop 60-3 (1)

Reliability & Quality
Assurance Office
Mail Stop 500-111 (1)

Technology Utilization Office
Mail Stop 3-19 (1)

Plans & Programs Office
Mail Stop 3-15 (1)

NASA Scientific & Technical
Information Facility
P. O. Box 5700
College Park, Maryland 20740

Attn: Acquisitions Branch
(SQT-34054) (1)

NASA Ames Research Center
Moffett Field, Calif. 94035

Attn. Library (1)

NASA Flight Research Center
P. O. Box 273
Edwards, California 93523

Attn. Library (1)

NASA Goddard Space Flight Center
Greenbelt, Maryland 20771

Attn. Library (1)

Jet Propulsion Laboratory
4800 Oak Grove Drive
Pasadena, California 91103

Attn. Library (1)

NASA Langley Research Center
Langley Station
Hampton, Virginia 23365

Attn. Library (1)

NASA Manned Spacecraft Center
Houston, Texas 77053

Attn. Library (1)

NASA Marshall Space Flight Center
Marshall Space Flight Center,
Alabama 35812

Attn. Library (1)

NASA Headquarters
Washington, D.C. 20546

Attn. N. F. Rekos (RAP) (1)
M. B. Comberiate (RAP) (1)

Aerojet-General Corporation
1100 West Hollyvale
Azusa, California 91702

Attn. Library (1)

Aerojet-General Corporation
Aerojet Liquid Rocket Company
Sacramento, California 98509

Attn: Library (1)
J. B. Accinelli (1)

Aerospace Corporation
P. O. Box 95085
Los Angeles, California 91745

Attn: Library (1)

AiResearch Manufacturing Company
402 South 36 Street
Phoenix, Arizona 85034

Attn: Library (1)
Lyle Six (1)

AiResearch Manufacturing Company
9851 Sepulveda Boulevard
Los Angeles, California 90009

Attn: Library (1)

Atomic Energy Commission
Division of Reactor Development
and Technology
Washington, D.C. 20767

Attn: N. Grossman (1)

Atomic Energy Commission
AEC-NASA Space Nuclear Propulsion
Office
Washington, D.C. 20545

Attn: N. Gerstein (1)

Avco Corporation
Lycoming Division
Stratford, Connecticut

Attn: Dr. M. Bentele (1)

Battelle Memorial Institute
Columbus Laboratories
505 King Avenue
Columbus, Ohio 43201

Attn: Library (1)
C.M. Allen (1)

Bell Helicopter Company
P. O. Box 482
Fort Worth, Texas 76101

Attn: C. Bowen (1)

Bendix Research Labs Division
Detroit, Michigan 48232

Attn: Library (1)

Boeing Company
Aerospace Division
P. O. Box 3707
Seattle, Washington 98124

Attn: Library (1)

Boeing Company
Vertol Division, Boeing Center
P. O. Box 16858
Philadelphia, Pennsylvania 19142

Attn: Library (1)
A. J. Lemanski (1)

Continental Aviation and
Engineering Corporation
12700 Kercheval Avenue
Detroit, Michigan 48215

Attn: Library (1)

Cornell University
Ithaca, New York 14850

Attn: Prof. J.F. Booker (1)

Curtiss-Wright Corporation
Wright Aero Division
Main & Passaic Streets
Woodridge, New Jersey 07075

Attn: Library (1)

Fafnir Bearing Company
37 Booth Street
New Britain, Connecticut 06050

Attn: R. J. Matt (1)

Franklin Institute Research Labs
Benjamin Franklin Pkwy. at 20th St.
Philadelphia, Pennsylvania 19103

Attn: W. Shapiro (1)

General Electric Company
Aircraft Engine Technical Div.
Bearings, Fuels & Lubricants
Evendale, Ohio 45215

Attn: E.N. Bamberger

General Electric Company
Flight Propulsion Division MD H25
Advanced Bearing & Seal Technology
Evendale, Ohio 45215

Attn: C.C. Moore (1)

General Electric Company
Mechanical Technology Laboratory
R&D Center
Schenectady, New York 12301

Attn: Library (1)

General Motors Corporation
Allison Division
Indianapolis, Indiana 46206

Attn: Library (1)

General Motors Corporation
New Departure - Hyatt Division
Hayes Avenue (Route 4)
Sandusky, Ohio 44871

Attn: B.T. Ruley (1)

Hughes Aircraft Corporation
Centinda & Teale Avenue
Culver City, California 90230

Attn: Library (1)

Industrial Tectonics, Inc.
18301 Santa Fe Avenue
Compton, California 90024

Attn: H. Hanau (1)

Institute for Defense Analyses
400 Army-Navy Drive
Arlington, Virginia 22202

Attn: Library (1)

Lockheed Missiles & Space Company
P. O. Box 504
Sunnyvale, California 94088

Attn: Library (1)

Massachusetts Institute of Technology
Cambridge, Massachusetts 02139

Attn: Library (1)

Mechanical Technology Incorporated
968 Albany-Shaker Road
Latham, New York 12110

Attn: Library (1)

Midwest Aero Industries, Corporation
4834 Delemere Avenue
Royal Oak, Michigan 48073

Attn: J.J. Sherlock (1)

National Science Foundation
Engineering Division
1800 G. Street, N.W.
Washington, D.C. 20540

Attn: Library (1)

Commanding Officer
Naval Air Propulsion Test Center
Philadelphia, Penn. 19112

Attn: AE, Bldg. 600-2
(James Conboy) (1)

Naval Air Systems Command
Propulsion Division
Jefferson Plaza, No. 2
Washington, D.C.

Attn: Robert R. Brown (1)

Naval Air Systems Command
Washington, D.C. 20360

Attn: S.M. Collegeman
AIR 5365A (1)

Naval Ship Engineering Center
Washington, D.C. 20360

Attn: W.C. Lindstrom
NSC 613D4B (1)

Naval Ship Research &
Development Center
Annapolis Division
Annapolis, Maryland 21402

Attn: W.V. Smith (1)

Naval Ship Systems Command
Washington, D.C. 20360

Attn: J.E. Dray
SNHIP 6148 (1)

North American Rockwell
Power Systems Divisions
6633 Canoga Avenue
Canoga Park, California 91304

Attn: Myles Butner (1)

North American Rockwell Corp.
Space Division
12214 Lakewood Boulevard
Downey, Calif. 90241

Attn: Library (1)

Office of Naval Research
Washington, D.C. 20360

Attn: S.W. Doroff ONR/463 (1)

SKF Industries, Incorporated
Engineering & Research Center
1100 First Avenue
King of Prussia, Penn. 19406

Attn: T. Tallian (1)
L. Sibley (1)

Sunstrand Denver
2480 West 70 Avenue
Denver, Colorado 80221

Attn: Library (1)

TRW Accessories Division
23555 Euclid Avenue
Cleveland, Ohio 44117

Attn: Library (1)

TRW Marlin Rockwell Division
402 Chandler Street
Jamestown, New York 14701

Attn: A.S. Irwin (1)

U.S. Army Engineering R&D Labs
Gas Turbine Test Facility
Fort Belvoir, Virginia 22060

Attn: W. Crim (1)

United Aircraft Corporation
Pratt & Whitney Aircraft Div.
400 Main Street
East Hartford, Conn. 06108

Attn: R. Shevchenko (1)
P. Brown (1)
Library (1)

United Aircraft Corporation
Sikorsky Aircraft Division
Stratford, Conn. 06497

Attn: Lester Burroughs (1)

University of Virginia
Dept. of Mechanical Engineering
Charlottesville, Virginia 22901

Attn: Prof. E.J. Gunter (1)

U.S. Army Aviation Materiels Labs.
Ft. Eustis, Virginia 23604

Attn: J.N. Daniel, SAVFE-AS (1)
L.M. Bartone, SAVFE-PP (1)